CHAPTER IV

Results and Analyses

4.1 The Stress Strain Responses from Triaxial Tests

It is widely recognized that the global stress-strain response during compression of a sand is dependent upon the initial density and initial mean effective stress. At a given stress level, initially dense specimens of sand will expand when sheared, while initially loose specimens will contract. The stress strain relationship from all tests; very loose, loose, medium and dense state with the confining pressure of 25, 50 and 80 kPa on D16, D40 and Silica test sand can be shown in Figure 4.1 - 4.3. It can be seen that the higher the confining pressure the higher the load carrying capacity of the soils. The abrupt drop of stress-strain curve after peak strength level could be observed in the dense specimens while there was no such sharp peak in the samples of loose condition. This stress drop always followed by the so-called softening behavior. This observed softening after each peak is a consequence of bifurcation instability in the vicinity of the peak. Dense specimens normally reached the peak state at the strains of about 2 - 5% depending on the initial condition of confining pressure. Namely the relatively high confining pressure slightly delayed the peak strength of the stress - strain response of the soils. The ultimate state would be generally reached after strains greater than 10%. On the other hand, most of the test sands in loose condition, especially with low confining stress, would compress throughout, shearing up to the ultimate state, no dominant peak could be observed. However, in a high confining stress, i.e. 80 kPa, some specimens exhibited a peak shear stress but the difference between this peak shear stress and corresponding ultimate stress was not as large as in the dense sample.

These observed behaviors are typical for loose and dense sands or normally consolidated and overconsolidated clays. Though this study did not measure the volumetric strain of the specimen, however, it could be recognized that sand in loose condition compresses as shear stress increases while sand in dense condition dilates

after a small compression. Because of the comparatively round shape of the grain, the Silica test sand has the smaller shear strength and starts failing at lower strain than D16 and D40 which have the angular shape of grain particle at the same packing condition and confining pressure. The somewhat round particle can easily rotate as well as slide when subjected to the surrounding pressure. However, Silica test sand shows the greater strain of ultimate strength compared to the other sands at the same initial state. The summary of the test results in terms of stress - strain value can be shown in Table 4.1.

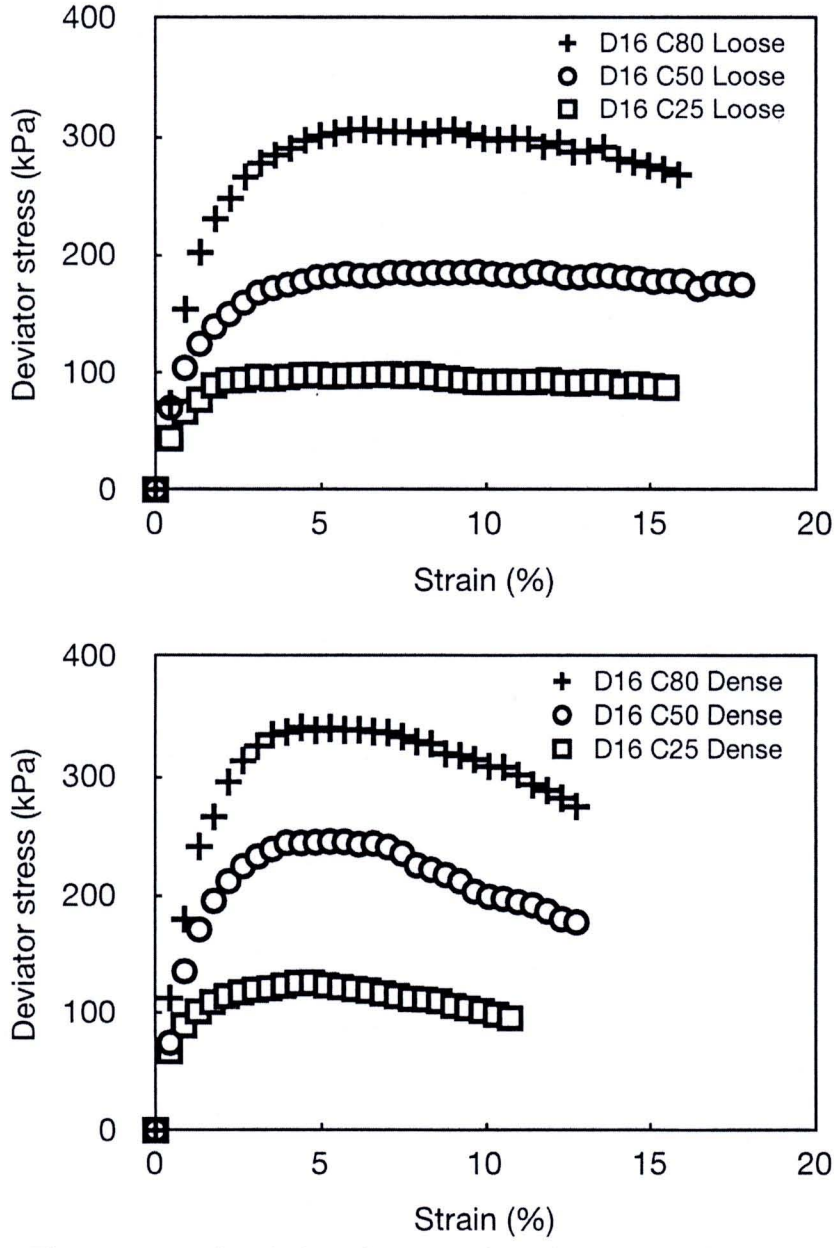

Figure 4.1 The stress - strain relation of D16 specimen in loose and dense conditions with confining pressure 80, 50 and 25 kPa

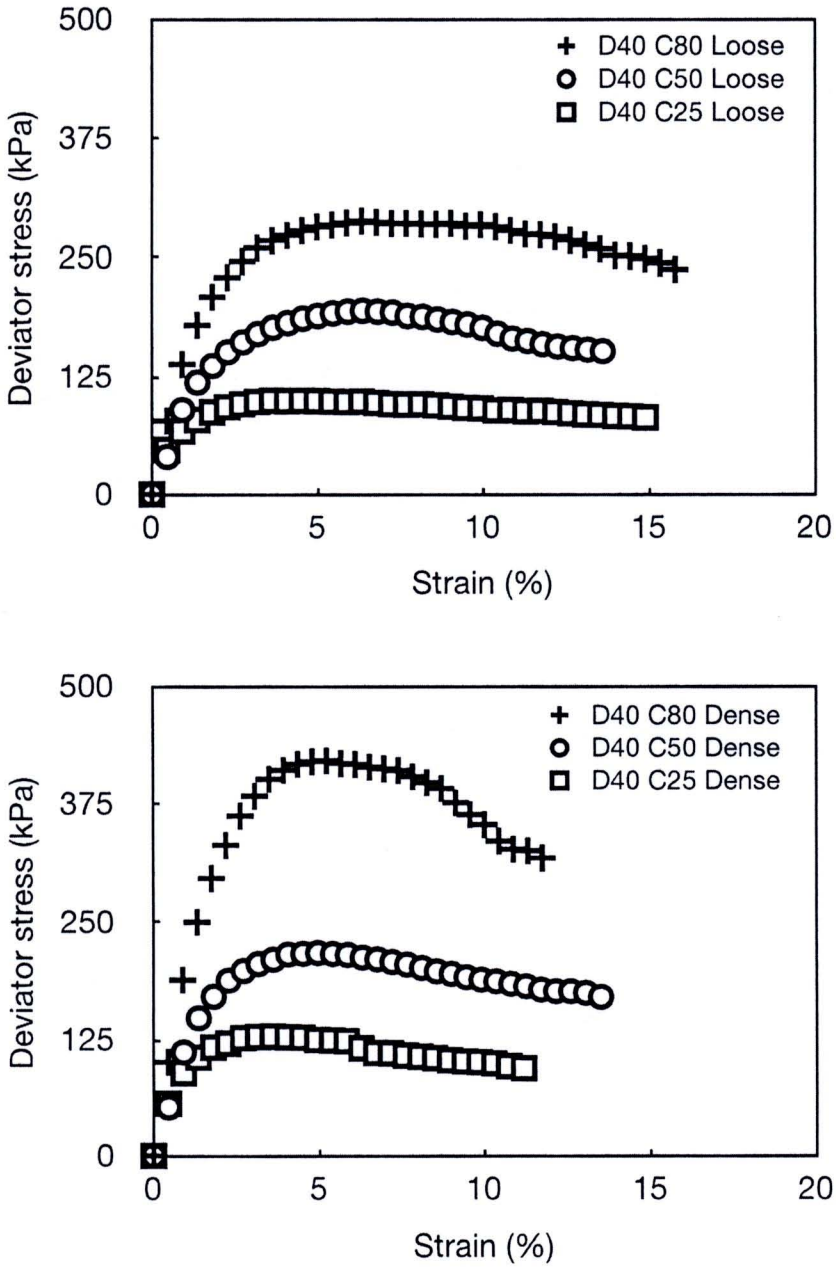

Figure 4.2 The stress - strain relation of D40 specimen in loose and dense conditions with confining pressure 80, 50 and 25 kPa

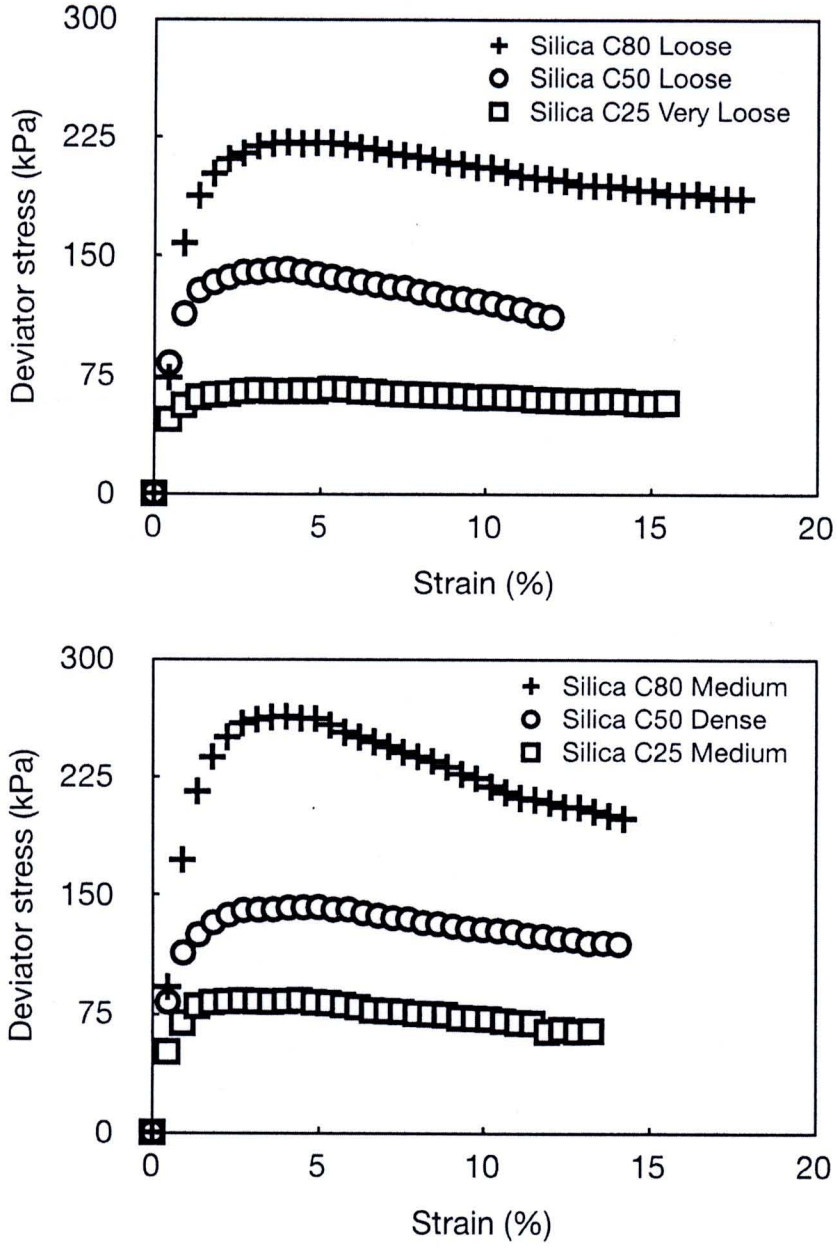

Figure 4.3 The stress - strain relation of Silica specimen in very loose, loose and dense conditions with confining pressure 80, 50 and 25 kPa

Table 4.1 Summary of the test results of stress - strain relationship

Initial condition	σ_c' (kPa)	Type of sand	Stress - strain characteristics			
			ε_1 (%) at peak	Max. q' (kPa)	ε_1 (%) at ultimate	Ultimate q' (kPa)
Loose	25	D16	4.42	98	15.47	87
		D40	3.61	99	14.87	81
		Silica[c]	5.30	67	15.45	58
	50	D16	5.87, 9.96[b]	184, 185[a]	18.11	174
		D40	5.89	194	13.60	152
		Silica	4.00	142	11.99	112
	80	D16	6.34	306	15.85	268
		D40	6.31	288	15.78	237
		Silica	3.54	221	17.68	186
Dense	25	D16	4.74	126	10.76	95
		D40	3.13	128	11.19	94
		Silica[d]	2.21	83	13.25	64
	50	D16	4.79	245	12.62	178
		D40	4.88	217	13.31	170
		Silica	4.99	143	14.07	119
	80	D16	4.40	341	12.77	275
		D40	5.22	421	11.75	318
		Silica[d]	4.00	264	14.21	199

σ_c' = confining pressure, ε_1 = axial strain and q' = deviator stress;
[a] represents an actual peak and [b] its corresponding strain;
[c] represents a very loose condition and [d] represents a medium condition

4.2 Shear Wave Velocity During Isotropic Loading and Shearing

4.2.1 Shear wave velocity under isotropic loading

Many researchers proposed the equations to correlate between V_s and state of stress in the direction of particle motion and wave proportion. Because sands are particulate materials, their V_s is governed by the mean state of stress (σ'_{mean}) in the polarization plane, where effective stress σ'_3 and σ'_1 act in the direction of particle motion and in the direction of shear wave propagation, respectively (Hardin and Richart, 1963). As a result, the V_s - stress relationship for granular material under isotropic loading (σ'_0) can be expressed as equation 4.1 by Santamarina *et al.* (2001):

$$V_s = \alpha \left(\frac{\sigma'_0}{1 \text{ kPa}} \right)^{\beta} \tag{4.1}$$

where α and β are experimentally determined from the in-situ or laboratory tested results. The α and β parameters represent the mechanical responses, i.e. contact effects, void ratio, coordination number, fabric change as well as the loading history. For a given soils, the α factor and β exponent can be uniquely estimated depending on the their porosity. The formulation of equation like in equation 4.1 for this studies can be shown by trend line of power function as in Figure 4.4 - 4.6 for D16, D40 and Silica sand samples in various initial state conditions. The values of α factor and β exponent of these testing results are plotted in the relationship, reproduced from Santamarina *et al.* (2001), between the typical value for α and β coefficients of clays, sands, steel balls and lead shot in order to observe the accuracy of the testing results obtained in the experiments (Figure 4.7). It can be discerned that the data from this studies moderately underestimates both α and β parameters compared to the linear correlation, equation 4.2, of those compiling data of various granular materials. However, the opposite trend between each other can be perceived in that such plots.

$$\beta = 0.36 - \frac{\alpha}{700} \tag{4.2}$$

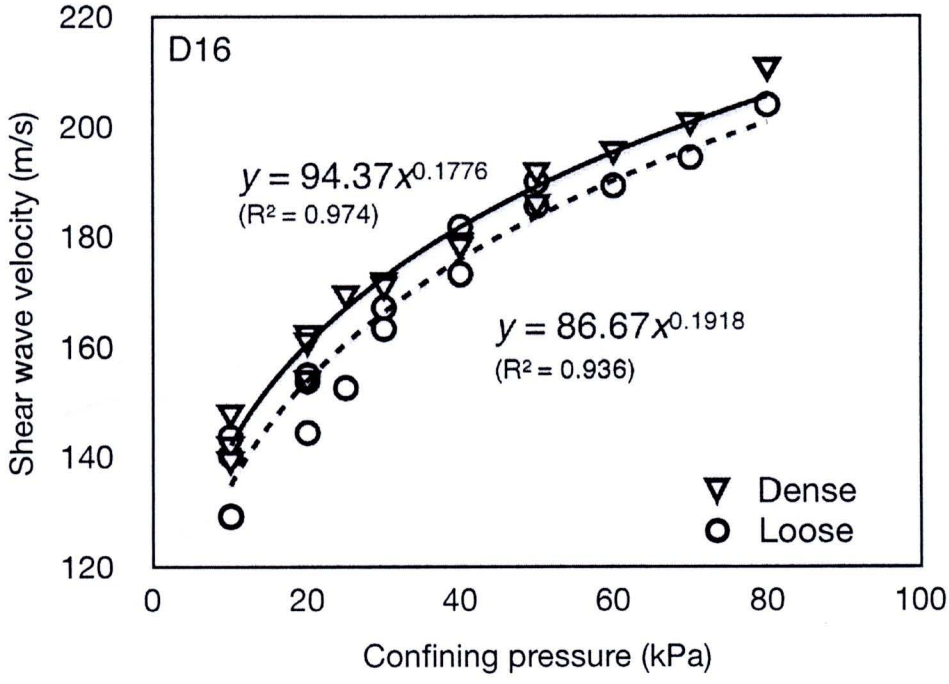

Figure 4.4 Shear wave velocity and stress relation of D16 sand in loose and dense conditions and its empirical relation

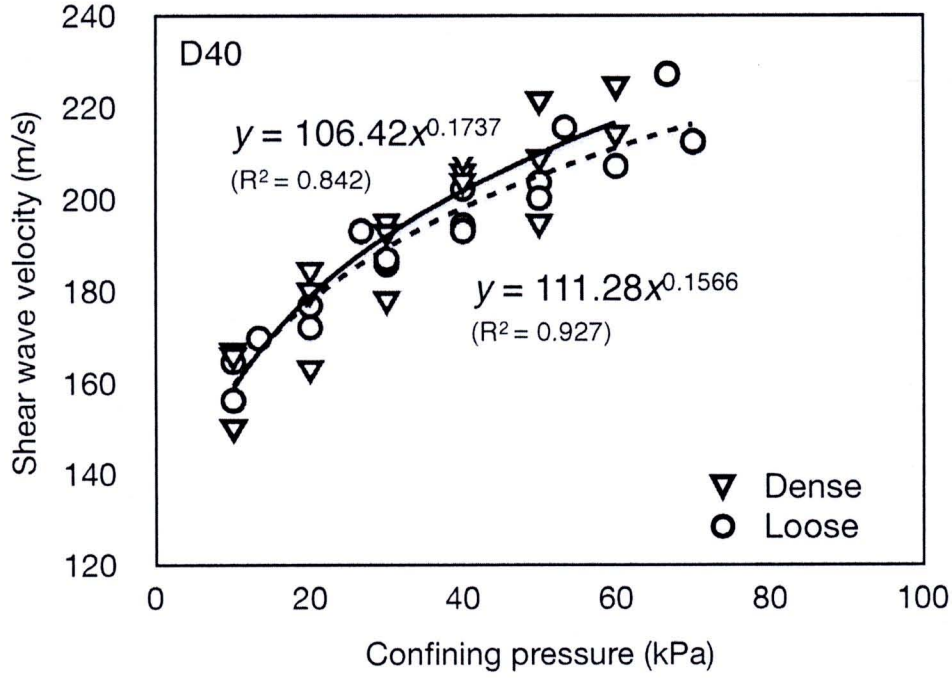

Figure 4.5 Shear wave velocity and stress relation of D40 sand in loose and dense conditions and its empirical relation

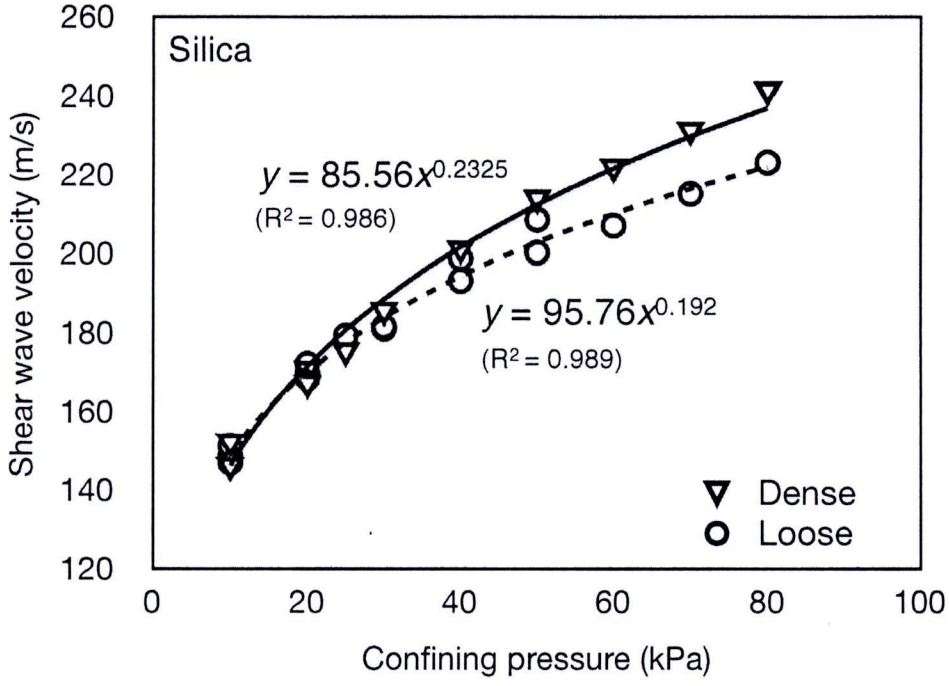

Figure 4.6 Shear wave velocity and stress relation of Silica sand in loose and dense conditions and its empirical relation

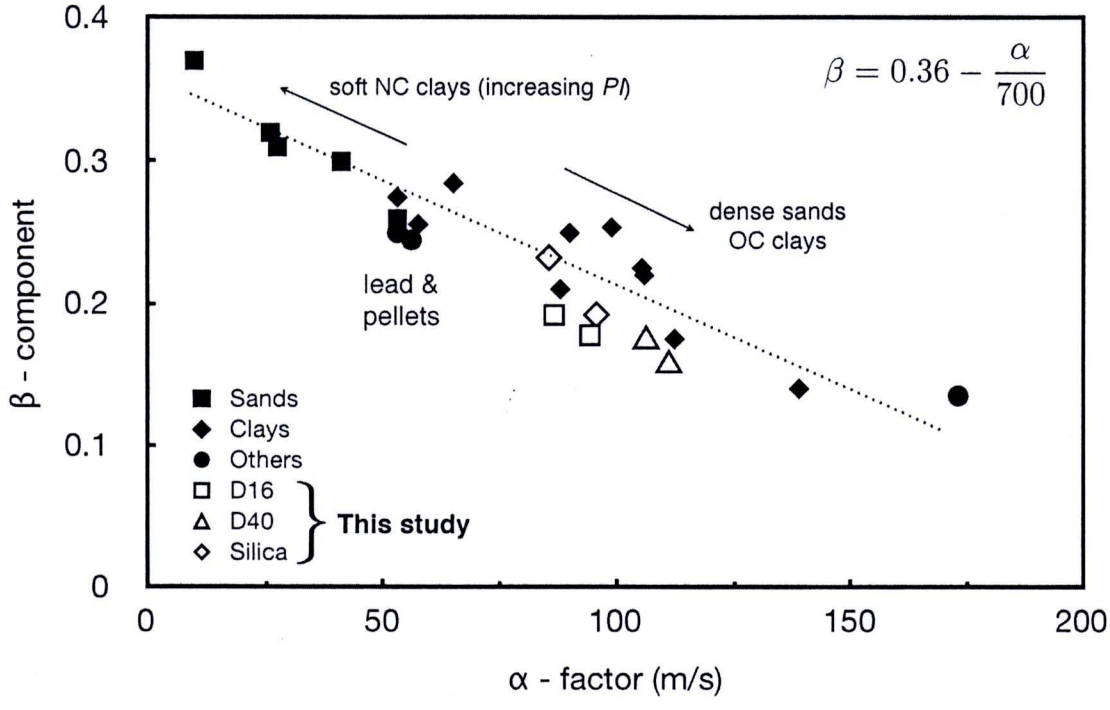

Figure 4.7 Typical values for α and β coefficients
(reproduced from Santamarina *et al.*, 2001)

However the value of α involves the influences of various properties, i.e. sample density as well as fabric characteristics. It is convenient to separate α factor into two new parameters; 1) A which includes the effect of grain properties and 2) $F(e)$ which includes the influence of packing properties, i.e. void ratio (e) and coordination number (C_n). Consequently, V_s that is measured within the same soil in various packing properties, e.g. loose and dense state, can be compared. Inversely, if we know V_s and their grain characteristic parameter, A, the porosity, n, or e can be empirically estimated. Equation 4.1 can be re-written as follows (Santamarina *et al.*, 2001):

$$V_s = AF(e)\left(\frac{\sigma_0'}{1\ \text{kPa}}\right)^{\beta} \tag{4.3}$$

The function $F(e)$ has been proposed for both sands and clays from the derivation of empirical formulas tested by various methods, e.g. resonant column, cyclic triaxial as well as ultrasonic pulse. The detailed formulation of this function can be found in Ishihara (1996). However, the classical proposed function (equation 4.4 and 4.5) by Hardin and Richard (1963) will be employed in this analysis.

$$F(e) = \frac{(2.17 - e)^2}{1 + e} \qquad \text{round particles} \tag{4.4}$$

$$F(e) = \frac{(2.97 - e)^2}{1 + e} \qquad \text{angular particles} \tag{4.5}$$

Figure 4.8 shows the variation between V_s and e of the D16, D40 and Silica sand in loose and dense conditions. This shear wave propagates within an elastic range of soil stress in an isotropic confining environment. It can be seen from this figure that the relatively linear correlation between V_s - e can be drawn though a scatter of data can be observed especially in the angular shape of soil grain, e.g. D16 and D40. Moreover, it can obviously conclude that the higher the void ratio the slower the shear wave velocity.

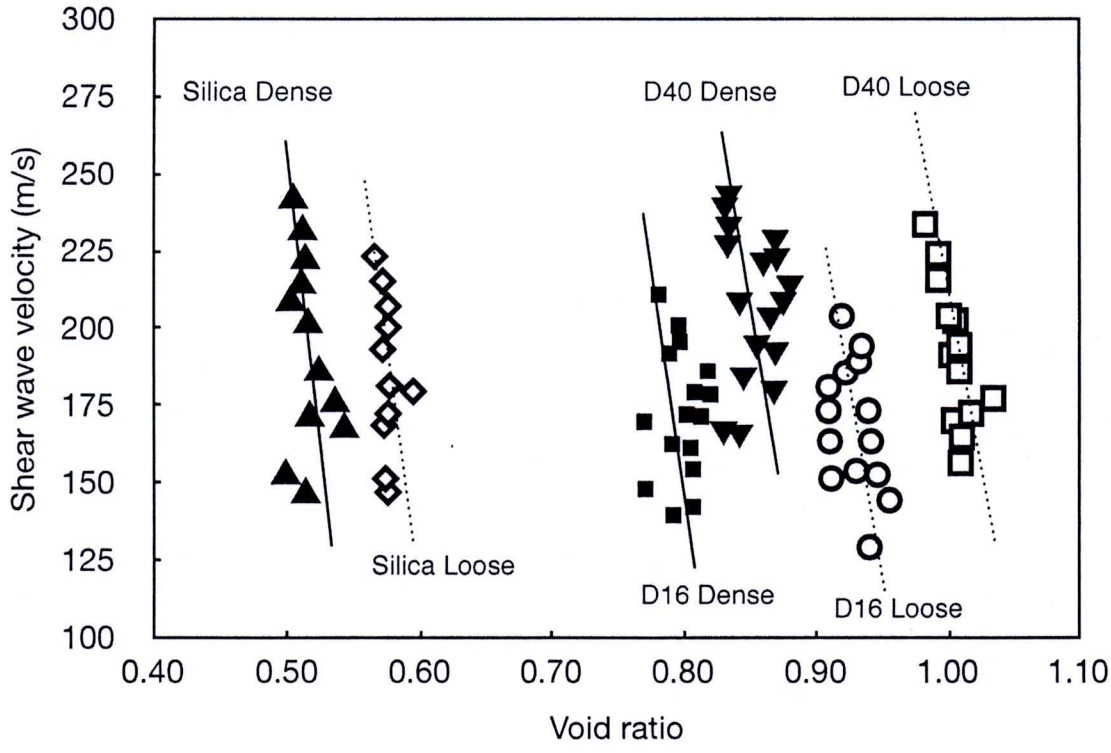

Figure 4.8 The variation between shear wave velocity and void ratio of D16, D40 and Silica sand in loose and dense conditions under isotropic loading

4.2.2 Shear wave velocity during shear

After required initial state of the test was attained, the sand specimen would be sheared by increasing the vertical load at a small rate of compression while the horizontal load would be kept to be constant by vacuum suction throughout the test. There are two empirical relations proposed in the literature to correlate between the V_s along the principle planes, x and y, with the stress in the direction of σ'_3 and σ'_1 which is the direction of particle motion and direction of wave propagation, respectively. Santamarina *et al.* (2001) complies those empirical formulas with the state of stress in anisotropically loaded media as follows;

$$V_s = \Omega \left(\frac{\sigma'_3}{1 \text{ kPa}} \right)^{\theta} \left(\frac{\sigma'_1}{1 \text{ kPa}} \right)^{\delta} \tag{4.6}$$

or

$$V_s = \Theta \left(\frac{\sigma_1' + \sigma_3'}{2 \text{ kPa}} \right)^{\zeta} \left(\frac{\sigma_1' - \sigma_3'}{2 \text{ kPa}} \right)^{\psi} \tag{4.7}$$

Similar to the empirical relationship of isotropically loading condition (equation 4.1), the coefficients Ω and Θ represent the void ratio of the arrangement at constant fabric as well as the packing property while the exponent constants θ, δ, ζ and ψ reflect the contact effect and the influence of fabric change. Those material parameters can be obtained in the experiments. Equations 4.6 and 4.7 will shorten to equation 4.1 in the isotropic state of loading.

Santamarina *et al.*, 2001 states that the effect of void ratio in coarse-grained materials, i.e. Ω and Θ, can also be separated to the function $F(e)$ as in equation 4.3. Nevertheless, this void ratio dependency is less relevant when the cohesionless materials were subjected to anisotropic loading due to fabric evolution and change in void ratio during shear. Santamarina and Cascante (1996) performed a resonant-column tests to observe the effect of isotropic and deviatoric stresses on wave propagation in paticulate materials at low strains as well as to interpret results at the micro level. The results of their experiment showed that the value of exponents θ and δ is in agreement with the exponent β obtained under isotropic loading, namely $\theta + \delta = \beta$. The stress acting in the direction of particle motion has a greater influence on V_s propagation (higher value of exponent parameter) than the stress in the direction of wave propagation. The exponent constants ζ and ψ of equation 4.7 were also regressed. The exponent ζ of the mean effective stress in the polarization plane is very similar to the isotropic exponent β. However, the exponent ψ for the deviatoric stress is close to zero ($\psi \approx 0$), i.e. -0.01 in axial compression, even when isotropic data was not considered in the regression analysis. Therefore it is sufficient to some extent, i.e. stress ratio less than 2 to 3, to calculate the V_s by considering only the mean state of stress in the polarization plane and the exponent for this mean stress equals to the exponent for isotropic loading, $\zeta = \beta$. The new equation as in equation 4.8 can be governed;

$$V_s = \Psi \left(\frac{\sigma'_{mean}}{1 \text{ kPa}} \right)^{\varphi} \tag{4.8}$$

where Ψ is the coefficient representing the effect of void ratio and φ is the exponent parameter reflecting the contact behavior under anisotropic loading environment of granular material. The figures illustrating the impact of σ'_{mean} to the V_s can be shown in Figure 4.9 - 4.11. It can be observed from those figures that the initial state of the sample, i.e. confining pressure and density condition has a few influences to the propagation velocity of shear wave. The grain size particle also impacts the shear wave propagation speed, the smaller the grain size the higher the V_s. This might be explained by the higher number of contact point of small grain size than large grain size. Moreover, at a certain value of σ'_{mean}, e.g. after starts shearing, the V_s drops continuously and the relationship as in equation 4.8 is not further valid due to the effect of strain localization.

The results from the triaxial compression test during shear in which the state of anisotropically loading takes place show that the influence of deviatoric stress, $(\sigma'_1 - \sigma'_3)$ is relatively low comparing to the influence of σ'_{mean} for all grain size of particles as well as packing conditions (Figure 4.12 - 4.14). This outcomes confirm the previous work by Santamarina and Cascante (1996) and the relationship of equation 4.8 that includes only the effect of σ'_{mean}. However, similar to the previous relationship between σ'_{mean} and V_s, at a certain level of shearing, i.e. principal stress ratio (q'/p') more than 1.2, the V_s deviates from its normal behavior, i.e. slowly increasing as the σ'_{mean} gets higher, as in equation 4.8. Namely, V_s stops increasing but tends to lessen and varies in some ranges before failure (Figure 4.15 - 4.17). This might be of course due to non-homogenous deformation as well as the initiation of the shear bands inside the specimen. The detailed discussion for this phenomena will be made later in the following section.

Figure 4.18 shows the example of shear wave propagation during isotropic consolidation and shear.

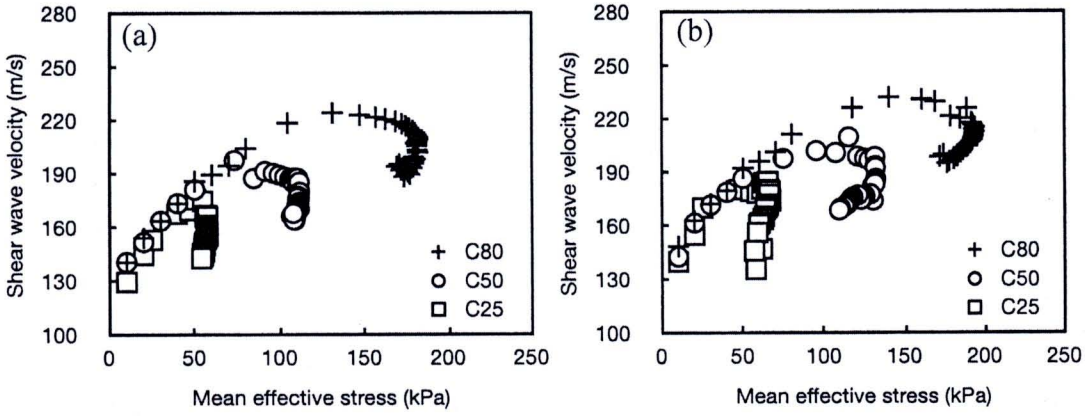

Figure 4.9 The influence of mean effective stress to shear wave velocity on D16 sample for a) loose and b) dense state in various confining conditions

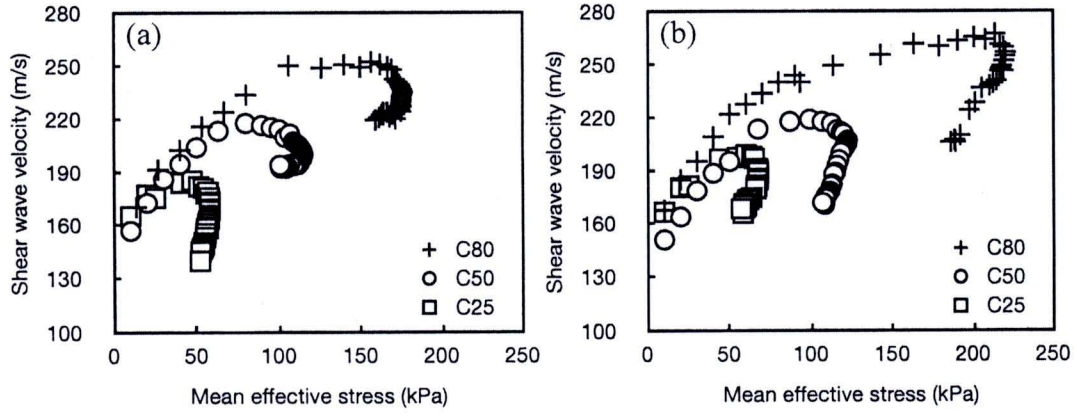

Figure 4.10 The influence of mean effective stress to the shear wave velocity on D40 sample for a) loose and b) dense state in various confining conditions

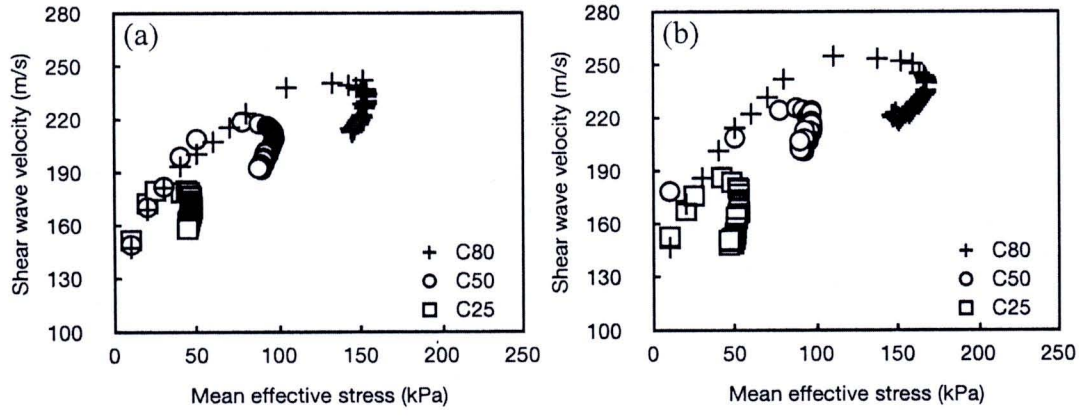

Figure 4.11 The influence of mean effective stress to the shear wave velocity on Silica sand for a) loose and b) dense state in various confining conditions

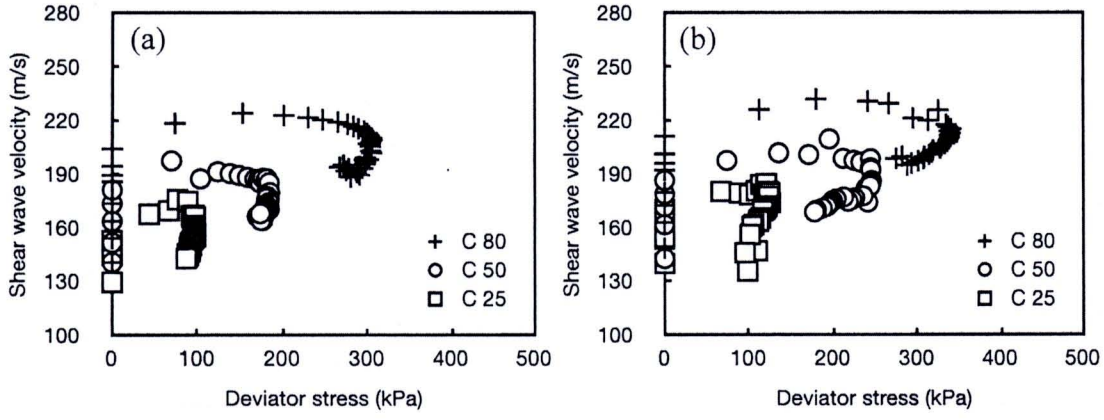

Figure 4.12 The influence of deviator stress to shear wave velocity on D16 sample for a) loose and b) dense state in various confining conditions

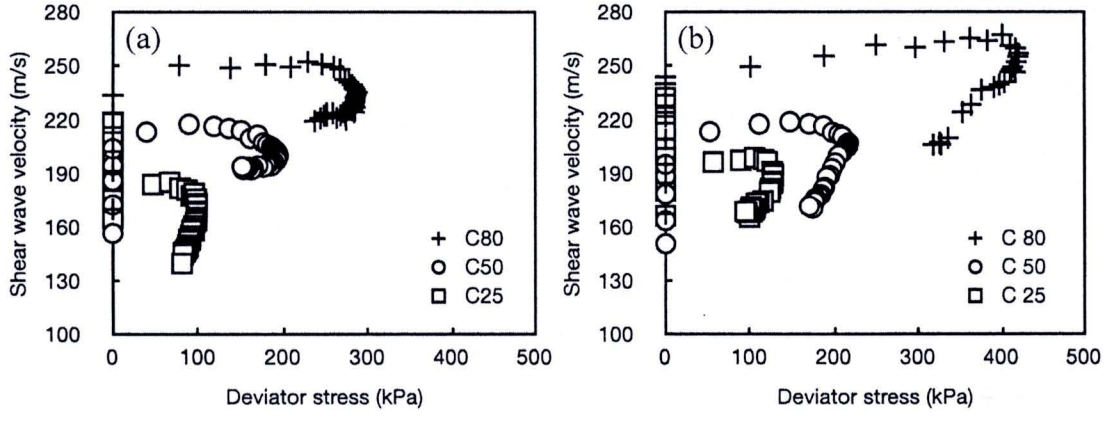

Figure 4.13 The influence of deviator stress to shear wave velocity on D40 sample for a) loose and b) dense state in various confining conditions

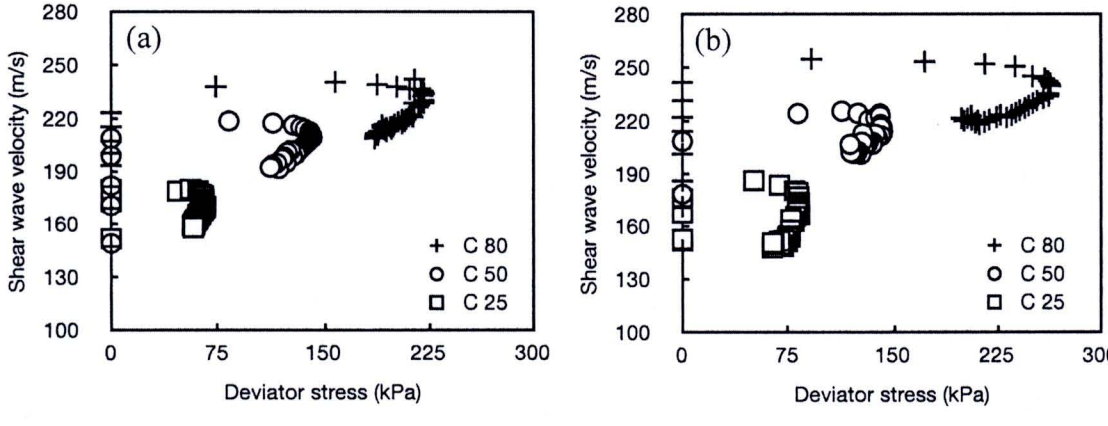

Figure 4.14 The influence of deviator stress to shear wave velocity on Silica sand for a) loose and b) dense state in various confining conditions

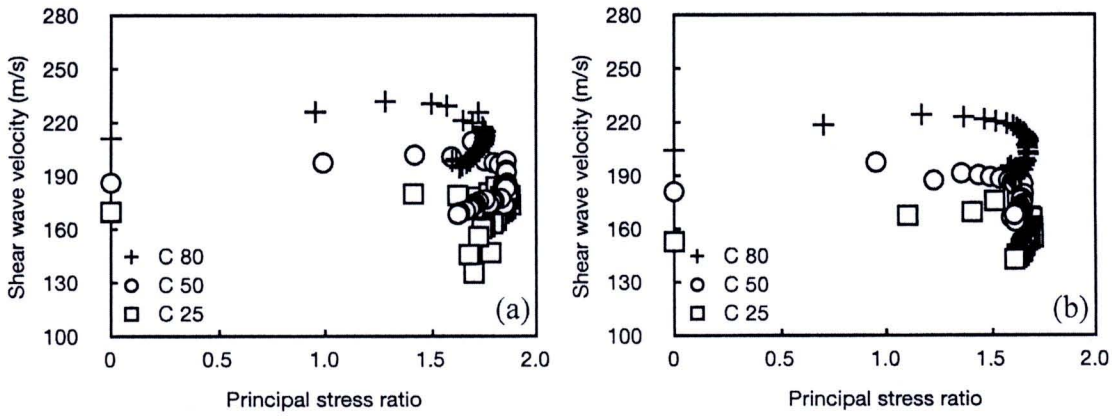

Figure 4.15 The variation between shear wave velocity and the principal stress ratio on D16 sample for a) loose and b) dense state in various confining conditions

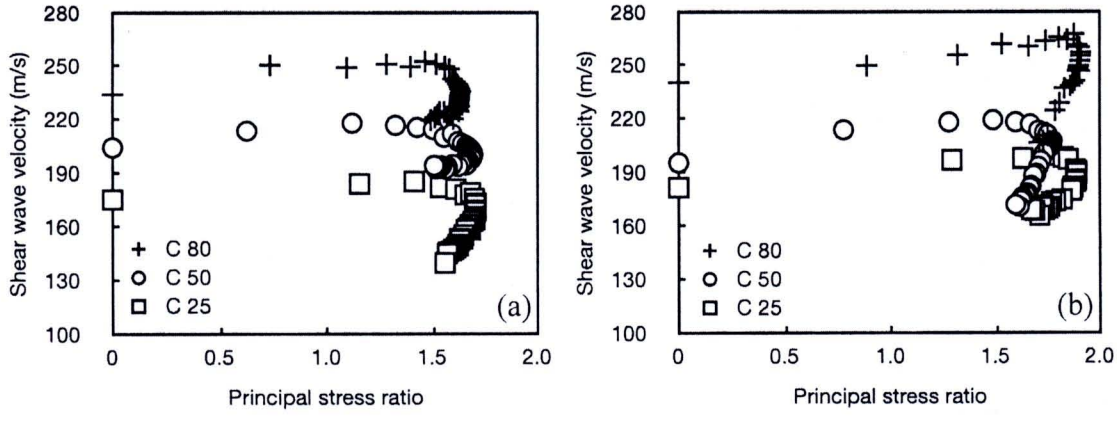

Figure 4.16 The variation between the shear wave velocity and the principal stress ratio on D40 sample for a) loose and b) dense state in various confining conditions

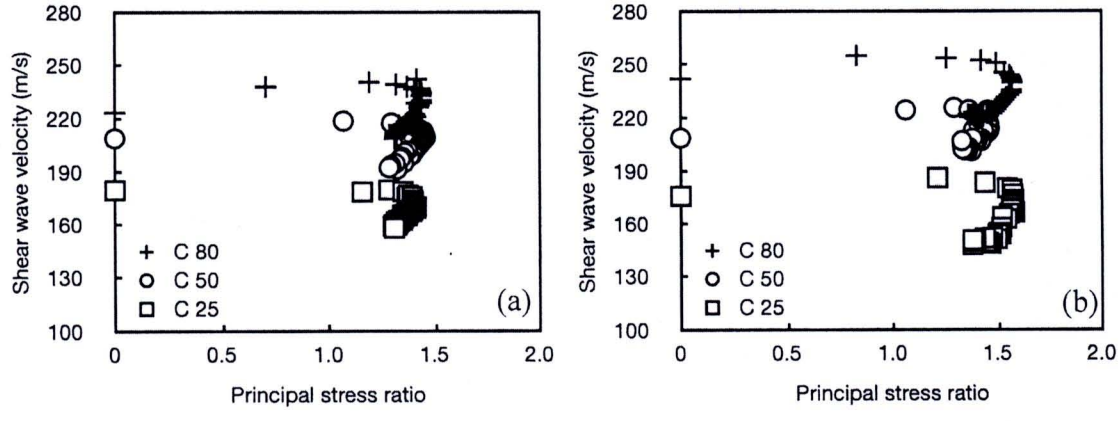

Figure 4.17 The variation between the shear wave velocity and the principal stress ratio on Silica sand for a) loose and b) dense state in various confining conditions

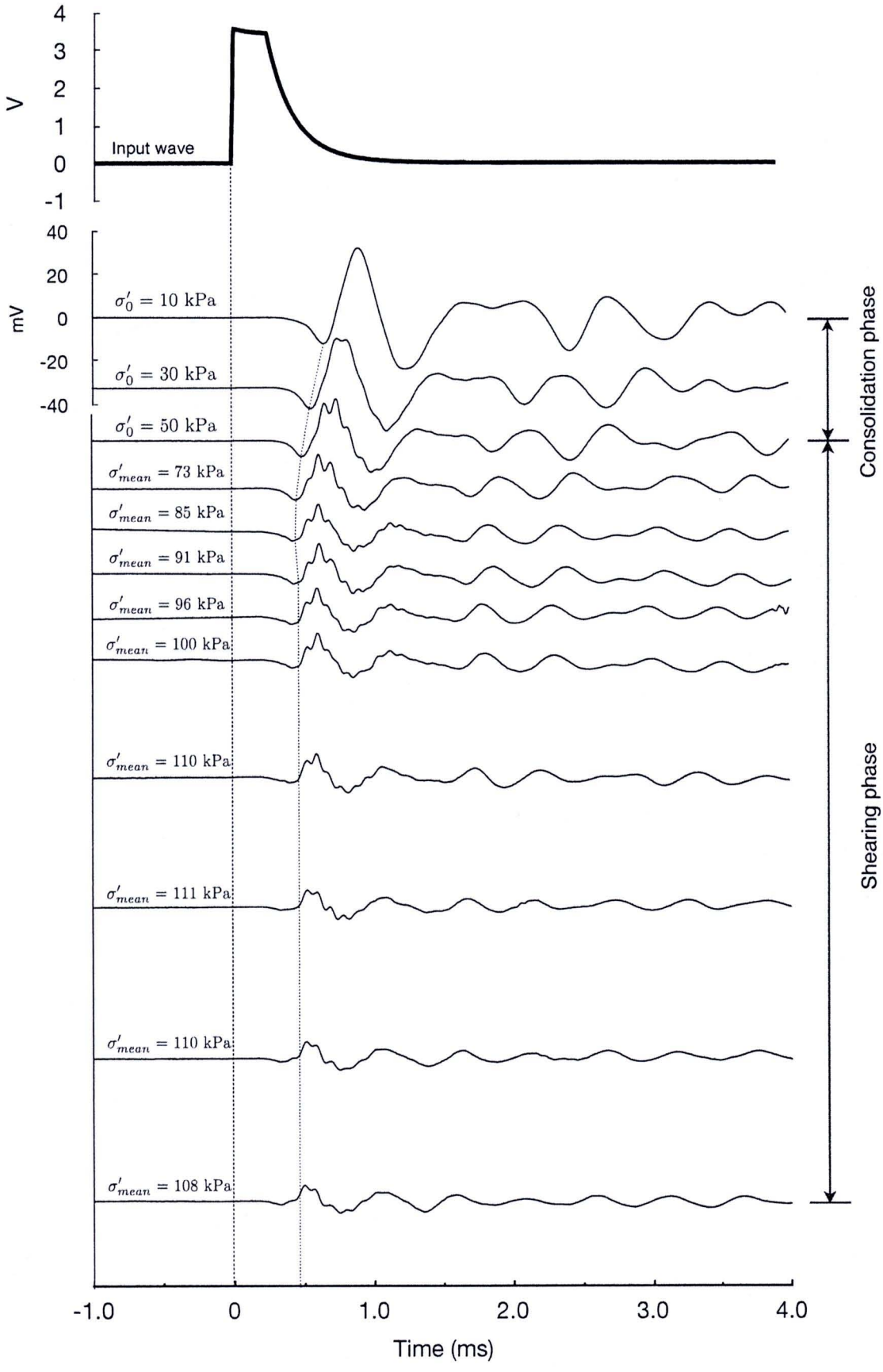

Figure 4.18 Shear wave propagation during isotropic consolidation and shear

4.3 The Initiation and Persistent of Strain Localization

4.3.1 Observation from shear wave velocity profile and stress ratio

There are a number of conclusions stating the onset and formation of shear band. Desrues and Viggiani (2004) inferred from their plane strain compression tests on sand that the onset of a persistent shear band will always occur near, i.e. at or slightly before, the peak of stress ratio and never occurs after that peak. Figure 4.19 shows an example of the stress strain responses in terms of effective stress ratio (t/s') vs global axial strain of biaxial test in sand and the stereophotogrammetry-based increment fields of shear strain intensity to explain that conclusions. From this figure, it can be seen that the progression of strain localization in test shf06 indicates the two parallel zones of strain localization form in the middle portion of the tested specimen in the increment 3-4, promptly prior to the peak of the stress ratio. It can also be perceived that though no shear bands were observed before increment 3-4, shear strain fields however suggest a somewhat non-homogeneous deformation presenting during an increment 2-3.

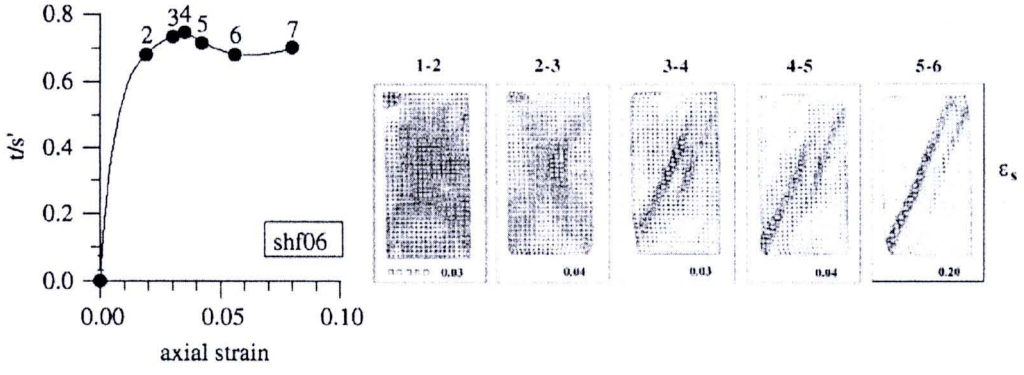

Figure 4.19 The effective stress ratio vs global axial strain of biaxial test in sand and the stereophotogrammetry-based increment fields of shear strain intensity (Desrues and Viggiani, 2004)

Finno *et al.* (1997) performed a series of plane strain compression on loose masonry sand. They concluded from the tested results that regardless of the drainage conditions, consolidated void ratio as well as mean effective stress, the friction mobilized when strain localization begins is very close to its maximum value. An

example of their results can be shown graphically in Figure 4.20. In this figure, we can see the lateral deformation response determined by the two pairs of horizontal linear variable displacement transducers (LVDTs). The local lateral strain at two elevations of the specimen is shown in images (a) and (b) while the absolute width difference between the upper and lower parts of the specimen and the sled or block movement are plotted in (c). Initially, the local lateral strain responses are parallel indicating a relatively uniform deformation. These responses ideally equal to the global axial strain (dashed line). However, based on the local lateral strain response, non-uniform deformation initiated at about 2.7% of global axial strain, as the two lateral strain responses begin to obviously diverge. This onset of non-homogeneous deformation is marked as point O. At approximately 3.6% global axial strain (marked as point B), the lateral strain rate of lower portion becomes almost zero (flatted growth) while the upper portion lateral strain rate increases to a constant value. They reported that at this point a shear band has bisected the specimen because deformations have concentrated in a zone of upper LVDT pair whereas no significant deformations are occurring in the zone bounded by the lower LVDT pair. They also found that the sled moves less than 0.3 mm until point O, then begins to move at a rate which becomes constant after 3.9% (point S). These results of lateral responses suggest a pattern of uniform deformation up to point O, followed by the progressive development of a shear band until point B which is the point that the band has completely developed.

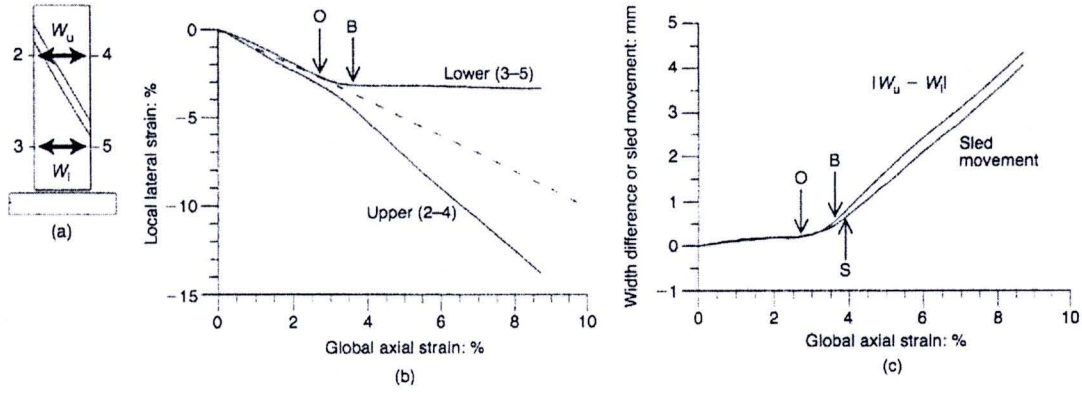

Figure 4.20 (a) The lateral deformation measurement (b) the lateral strain vs the global axial strain at two elevations (c) the absolute width difference between the upper and lower parts of the specimen and the sled or block movement (Finno *et al.*, 1997)

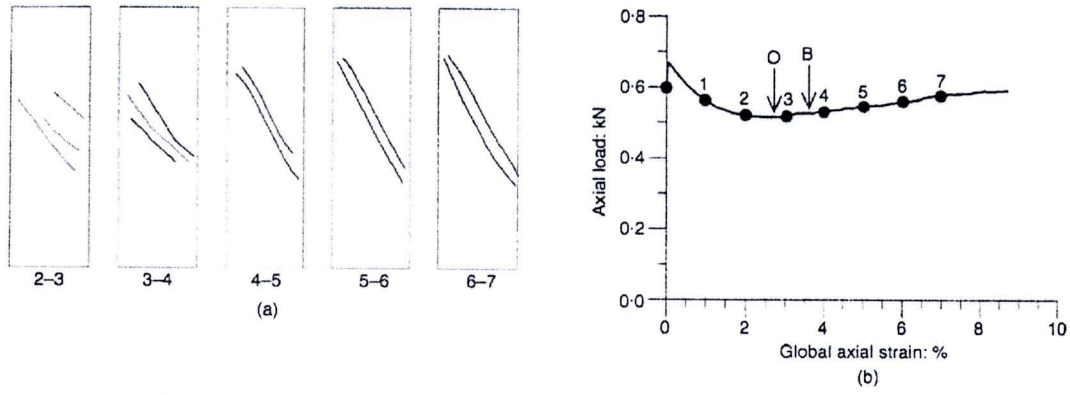

Figure 4.21 Evolution of shear bands (a) images from intervals of global axial strain by stereo-comparison (b) axial load curve (Finno *et al.*, 1997)

They explained from the above figure that while no localization of strain was observed in the test before 2% of global axial strain, a wide zone of slight strain localization appears in the middle portion of the specimen when photographs at 2% and 3% are viewed in stereo. In the subsequent increment 3-4, this zone becomes steeper and narrower, meaning that the shear strains are larger and more localized. A single shear band is clearly observed in increment 4-5 and is maintained throughout the test. To further quantify the progression of shear band formation, points O and B were specified in the axial load curve. While point B is clearly defined by the achievement of constant rates of local lateral strain, the selection of point O is relatively subjective. However, the occurrence of strain localization in increment 2-3 corroborates the selection of point O at approximately 2.7%. The results from the lateral deformation response (Figure 4.20) together with stero-comparison (Figure 4.21) can ably present a consistent account of the strain localization development inside the soil sample. The stress strain response during shear is also presented in Figure 4.22 in terms of effective principal stress ratio (q'/p') against global axial strain. The mobilized friction q'/p' monotonically increases to a peak at 1.13 (point F), then slightly decreases to a constant value of 1.10. This maximum friction mobilized after the onset of non-homogeneous deformation at point O, whereas the band is completely formed (point B) just after point F.

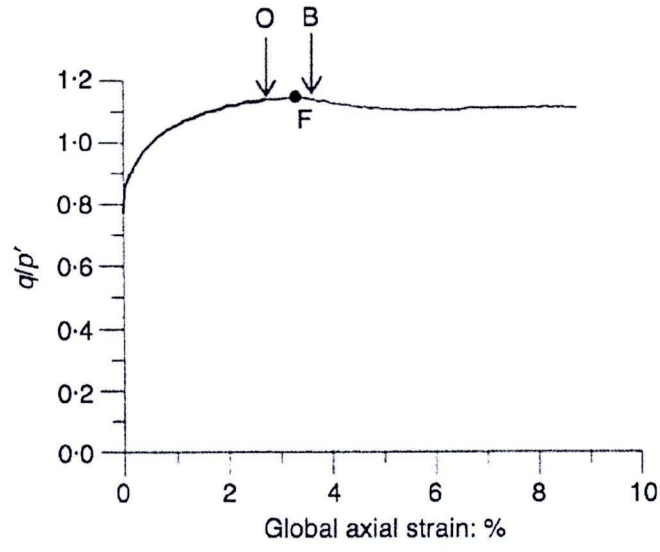

Figure 4.22 Stress strain response in terms of stress ratio during shear (Finno *et al.*, 1997)

From the example of above reports and conclusions in the biaxial tests, for triaxial test results in clays see in Sachan and Penumadu (2007), we can understand that the progression of strain localization takes place in the tested specimens at or shortly prior to the mobilization of peak friction following the fairly uniform vertical (axial) compression coupled with slight lateral expansion. After the achievement of this peak stress, the failure planes in the form of significant multiple shear bands, later developing to a single band, are presented in the post peak response.

Figures 4.23 to 4.40 show the relationship between effective stress ratio (q'/p') versus axial strain which is similar to the previous plot of above researches together with the plot of complete V_s profile against axial strain of triaxial compression test. The typical results of these figures in terms of effective stress ratio as well as the profile of V_s propagation inside the specimen during the entire compression test are depicted in Figure 4.41. It is clearly recognized from the testing results and analyses in the previous sections and in figure 4.41a and 4.41b that V_s in the consolidation state and in the very beginning part of shearing state, i.e. axial strain less than 2%, remarkably increases as σ'_0 or σ'_{mean} increases. The higher the confining pressure, the higher the increasing in V_s. This nonlinear relation is only valid within an elastic range of both isotropic (consolidation state) and anisotropic (shearing state) loading conditions. After soils reach a yield point which is the point of

transformation from the uniform to non-uniform state, V_s tends to grow slowly. The point of material yield is a marked change in the gradient of a stress-strain curve. This is associated with a fundamental change in behavior often from elastic and recoverable straining to inelastic and irrecoverable straining. This yield point in the stress-strain curve corresponds to the first Maximum Shear Wave Velocity (MVS_f) during the compression test in this analysis. Moreover, sands with relatively more angular shape, e.g. D16 and D40, due to their inherent characteristic to withstand sliding and rolling of particle movements can a little bit develop the shear wave propagation to a certain value. Namely, the maximum shear wave velocity (MVS) can reach the higher value than the first one (MVS_f). In contrast, the results of Silica sand always exhibit the same point between MVS_f and MVS. After the point of MVS the V_s for all tests reduces linearly and remains relatively constant from a particular point of large axial strain. This tendency to some extent confirms the non-uniformity and the initiation of strain localization inside the specimen because V_s is not further a function of void ratio and stress state. It can also be explained that this reduction of V_s is independent on particle shape and size but is dependent on the initial condition of the sample. In other words, dense sample manifests higher downslope than the loose one. This reduction of V_s can be explained by 2 main reasons; 1) the lowering of specimen height during shear and 2) the development of strain localization inside the sample.

Although the maximum stress ratio (MSR) comparatively varies among a specific range of strain but it is rational to note that the lower the initial confining pressure the earlier the mark of MSR. Moreover, at the point of MSR there is no remarkable change in V_s. It is therefore difficult to detect that which point is the initiation point of strain localization inside the soil mass.

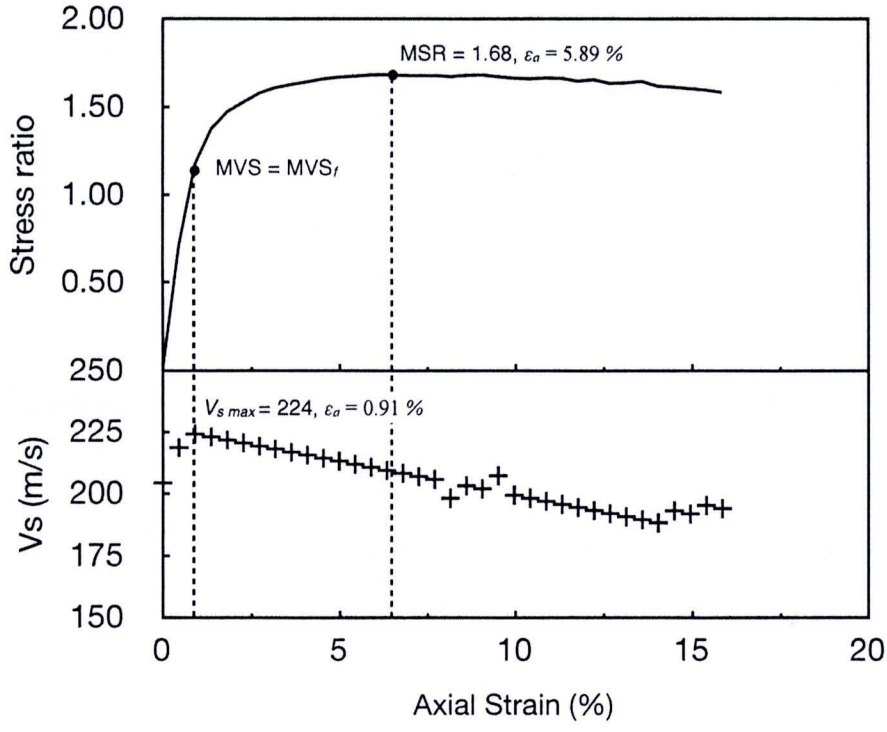

Figure 4.23 The stress ratio and shear wave velocity (V_s) against strain for D16 in loose condition with confining pressure 80 kPa

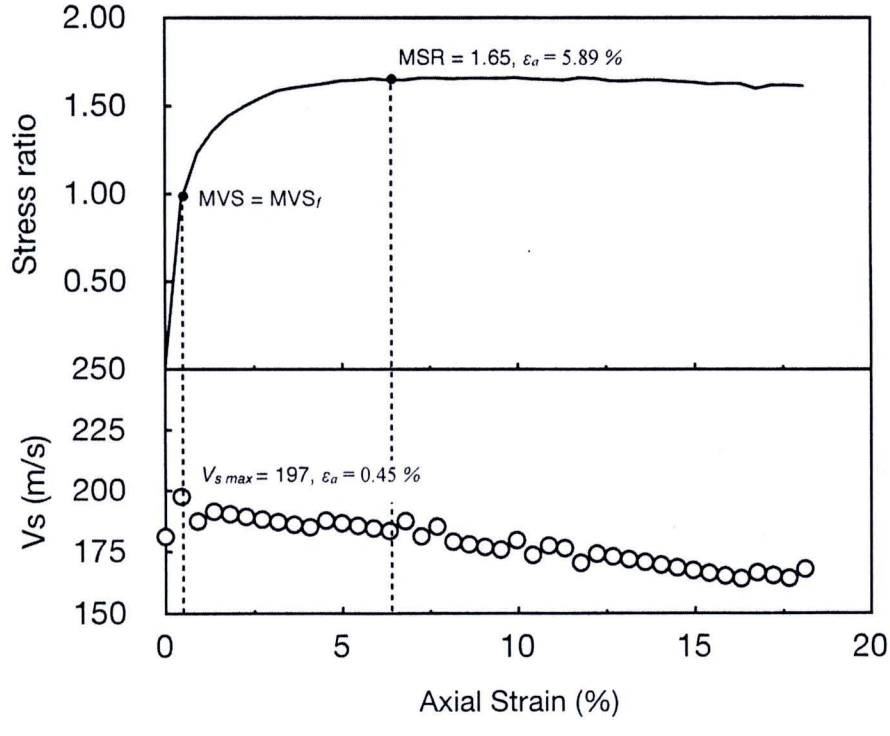

Figure 4.24 The stress ratio and shear wave velocity (V_s) against strain for D16 in loose condition with confining pressure 50 kPa

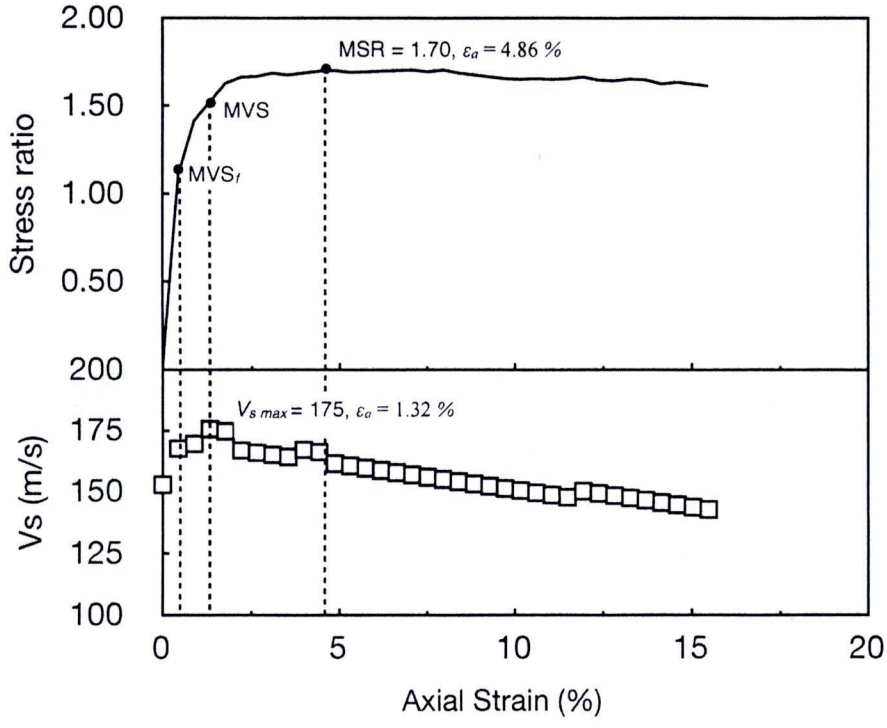

Figure 4.25 The stress ratio and shear wave velocity (V_s) against strain for D16 in loose condition with confining pressure 25 kPa

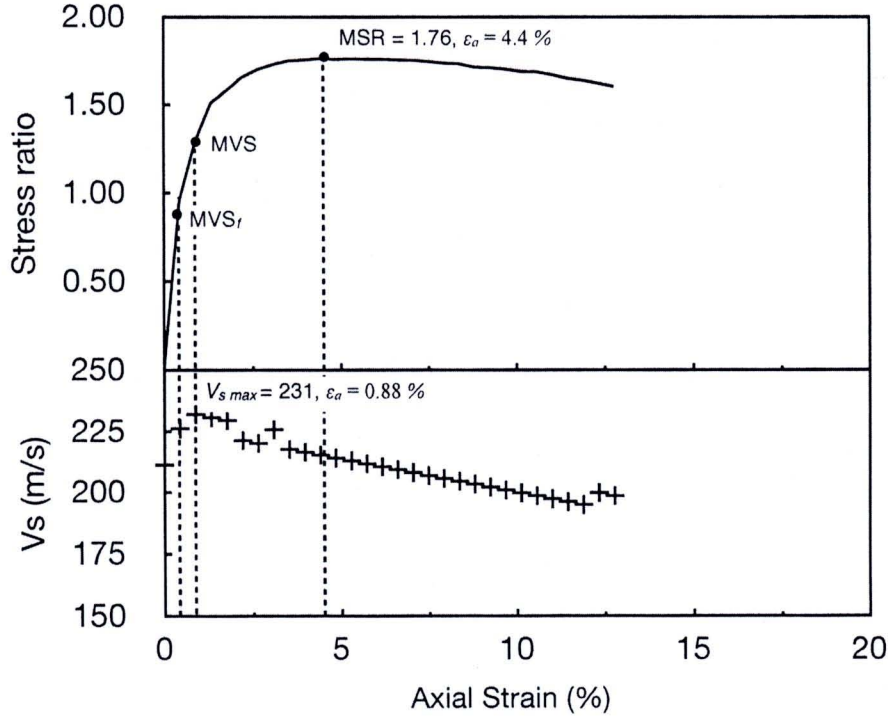

Figure 4.26 The stress ratio and shear wave velocity (V_s) against strain for D16 in dense condition with confining pressure 80 kPa

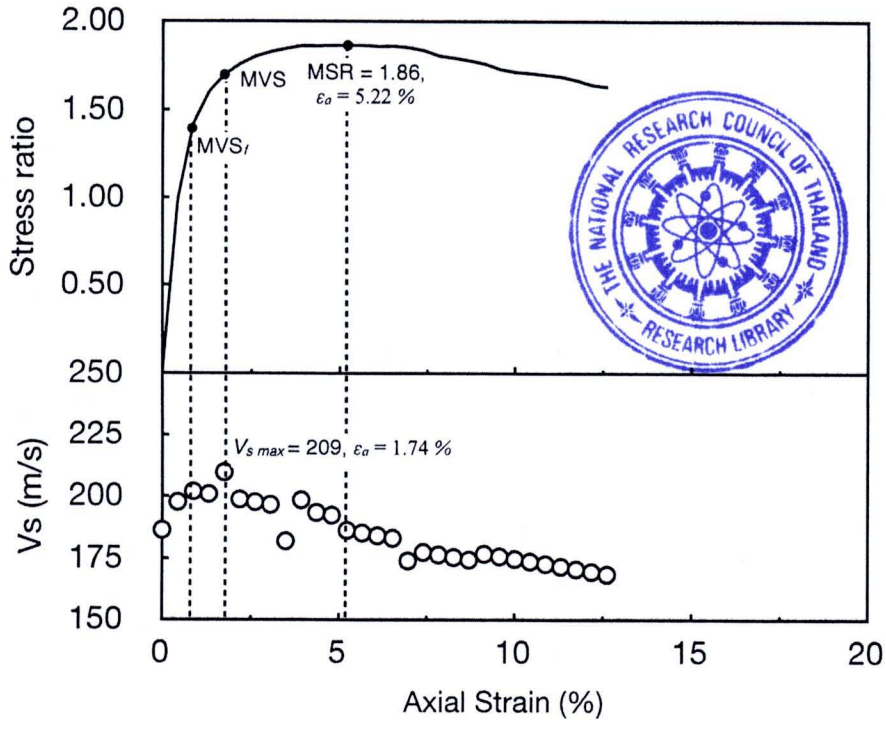

Figure 4.27 The stress ratio and shear wave velocity (V_s) against strain for D16 in dense condition with confining pressure 50 kPa

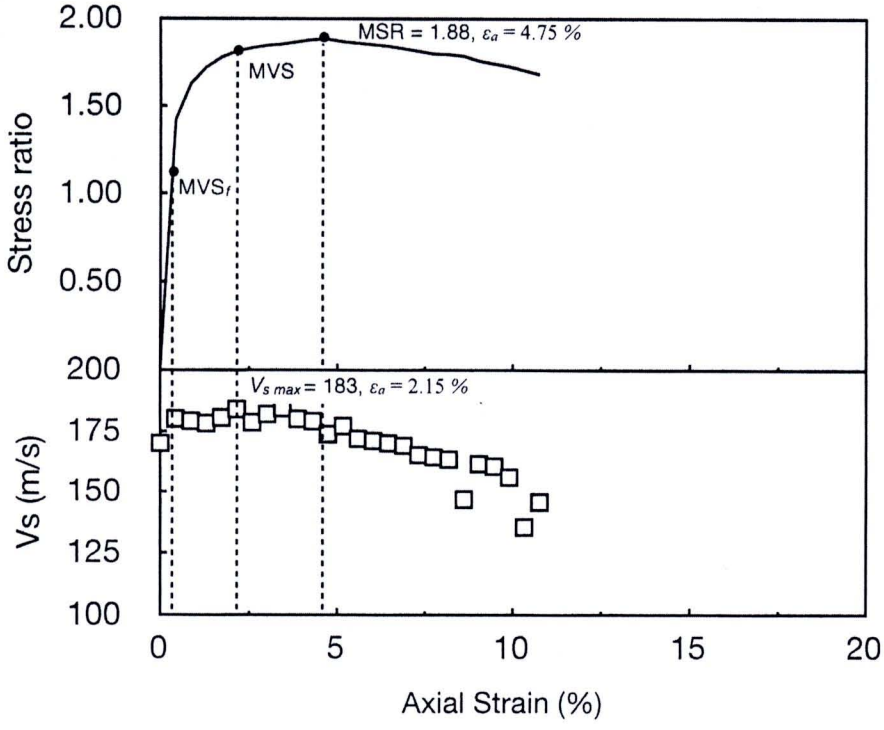

Figure 4.28 The stress ratio and shear wave velocity (V_s) against strain for D16 in dense condition with confining pressure 25 kPa

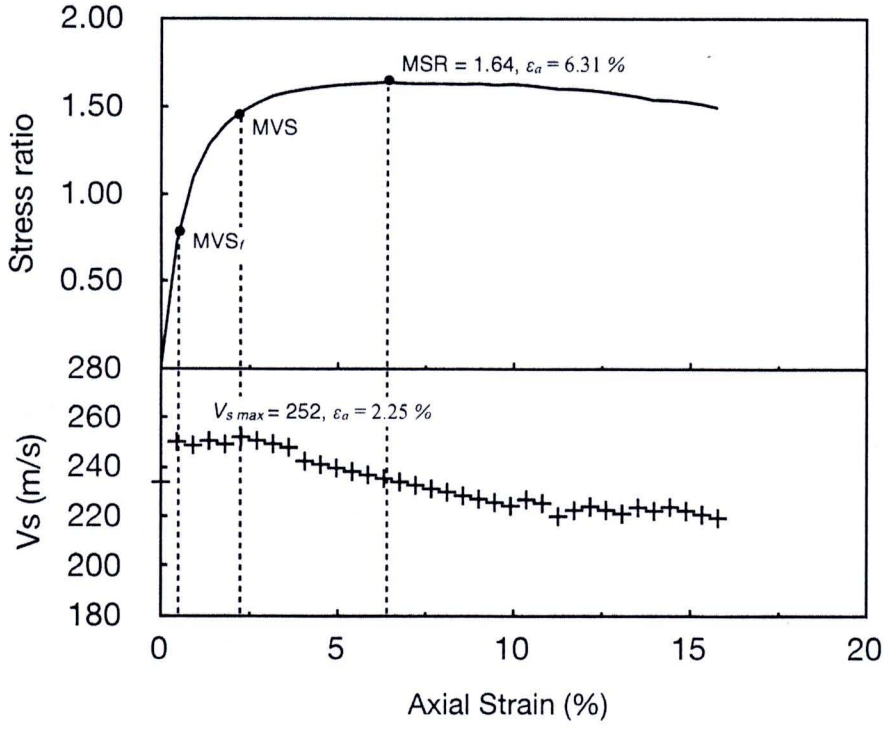

Figure 4.29 The stress ratio and shear wave velocity (V_s) against strain for D40 in loose condition with confining pressure 80 kPa

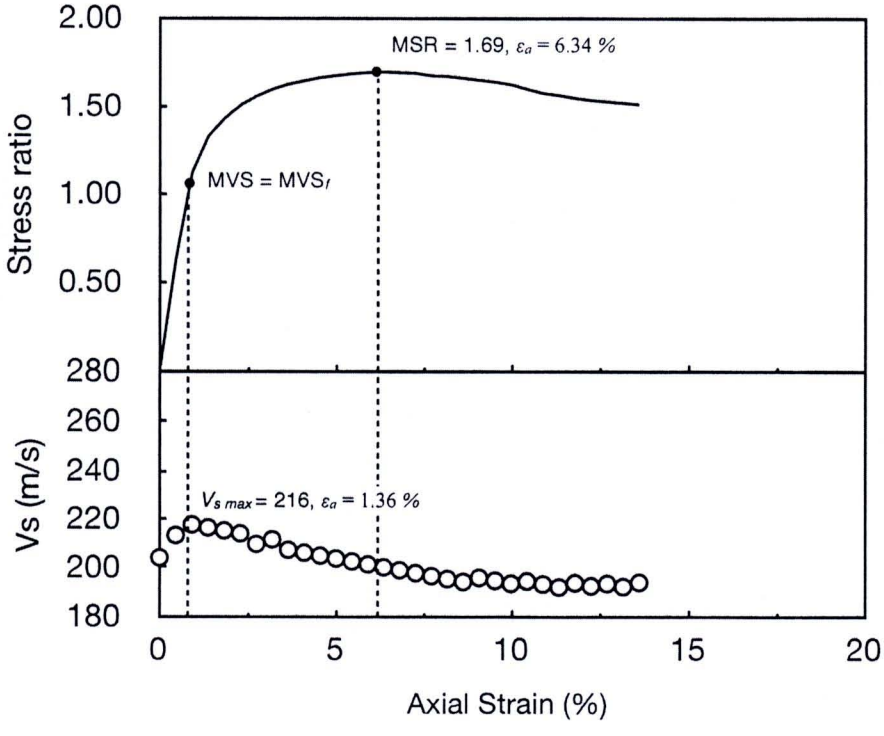

Figure 4.30 The stress ratio and shear wave velocity (V_s) against strain for D40 in loose condition with confining pressure 50 kPa

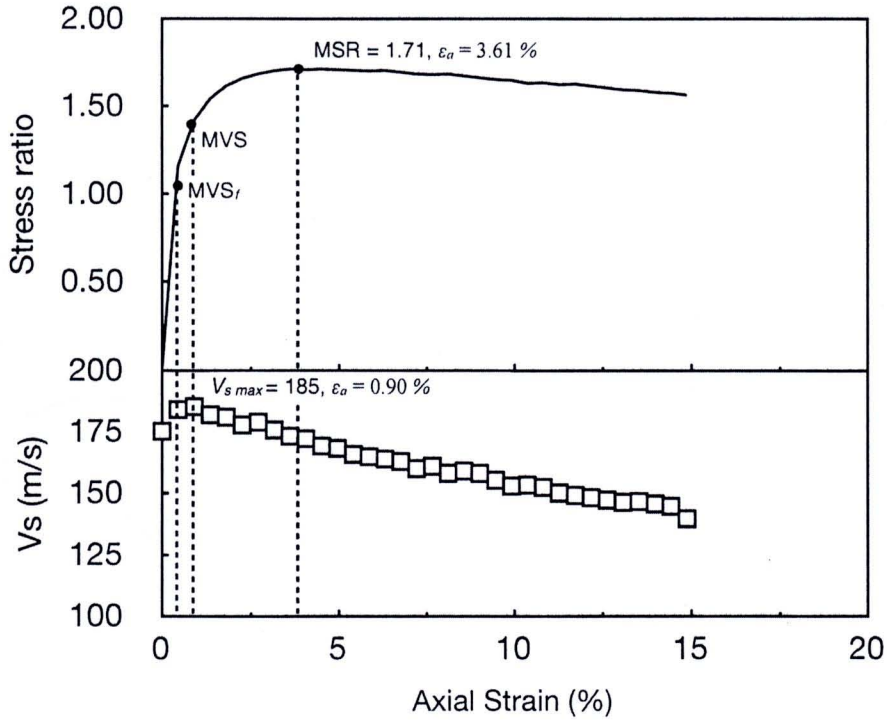

Figure 4.31 The stress ratio and shear wave velocity (V_s) against strain for D40 in loose condition with confining pressure 25 kPa

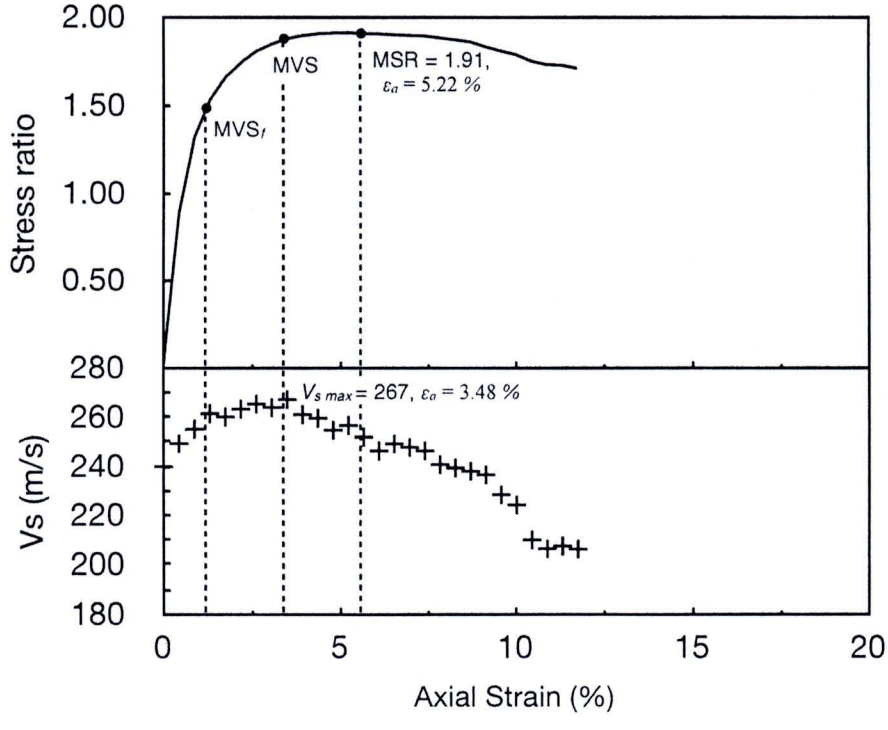

Figure 4.32 The stress ratio and shear wave velocity (V_s) against strain for D40 in dense condition with confining pressure 80 kPa

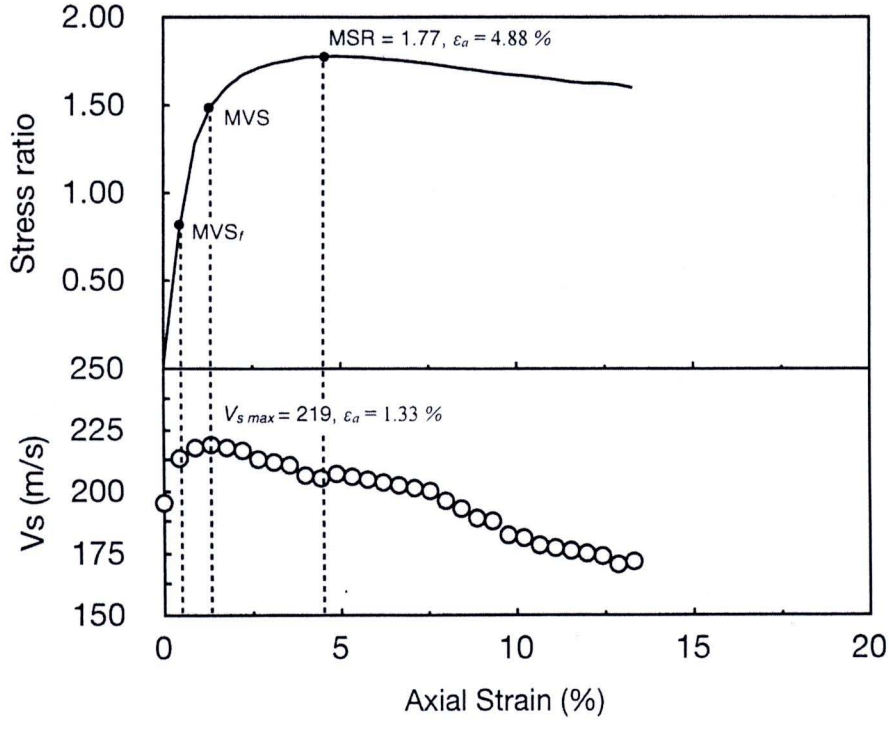

Figure 4.33 The stress ratio and shear wave velocity (V_s) against strain for D40 in dense condition with confining pressure 50 kPa

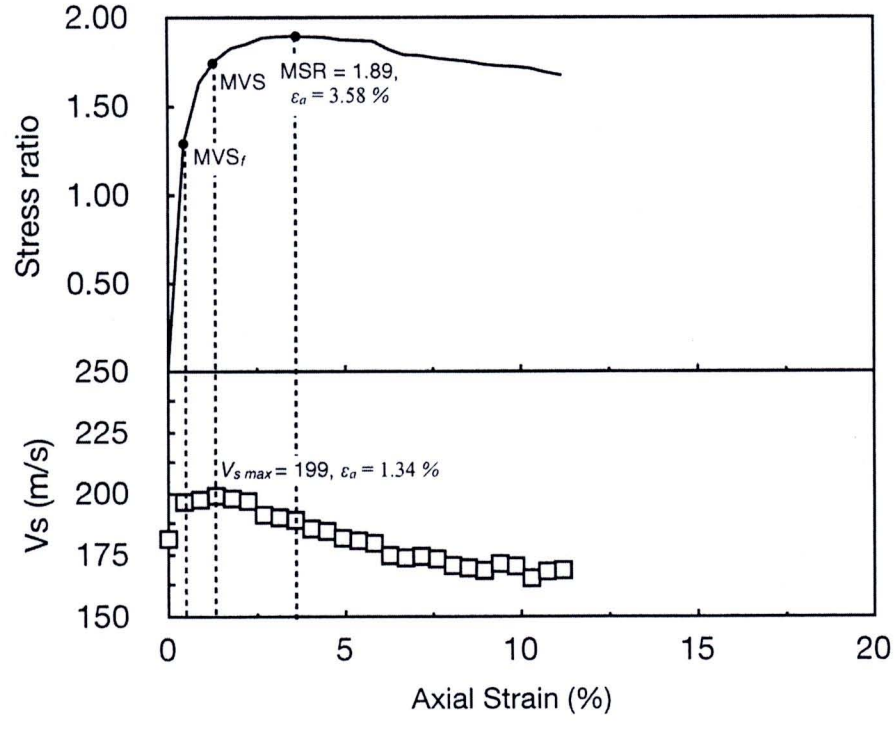

Figure 4.34 The stress ratio and shear wave velocity (V_s) against strain for D40 in dense condition with confining pressure 25 kPa

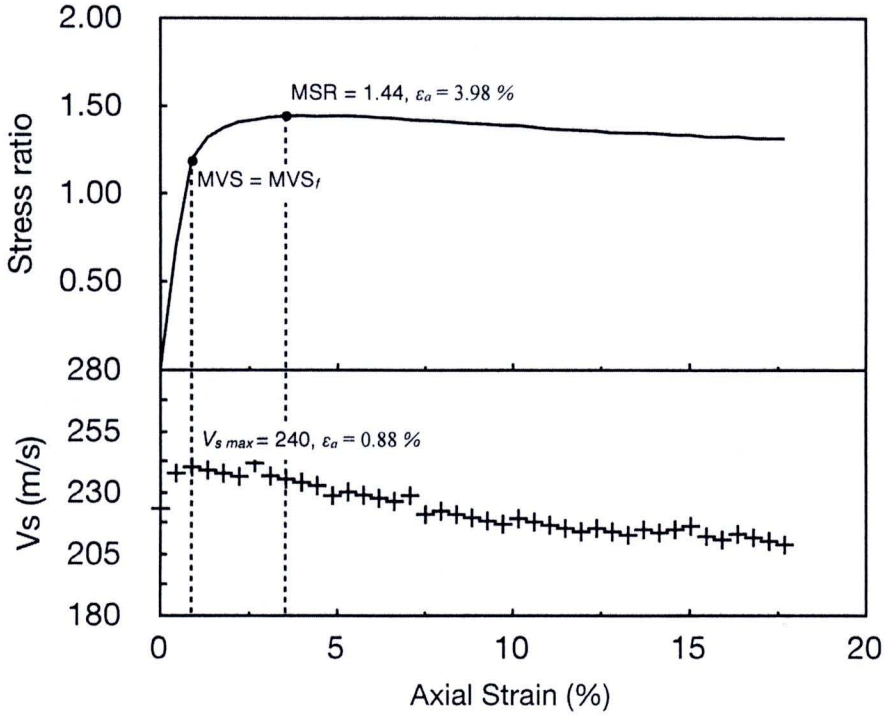

Figure 4.35 The stress ratio and shear wave velocity (V_s) against strain for Silica sand in loose condition with confining pressure 80 kPa

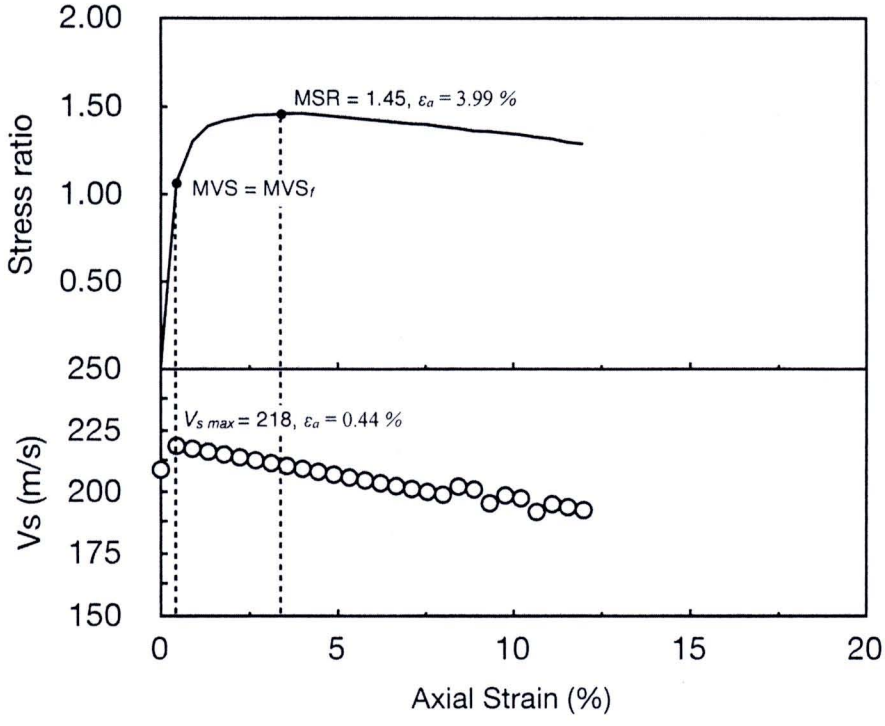

Figure 4.36 The stress ratio and shear wave velocity (V_s) against strain for Silica sand in loose condition with confining pressure 50 kPa

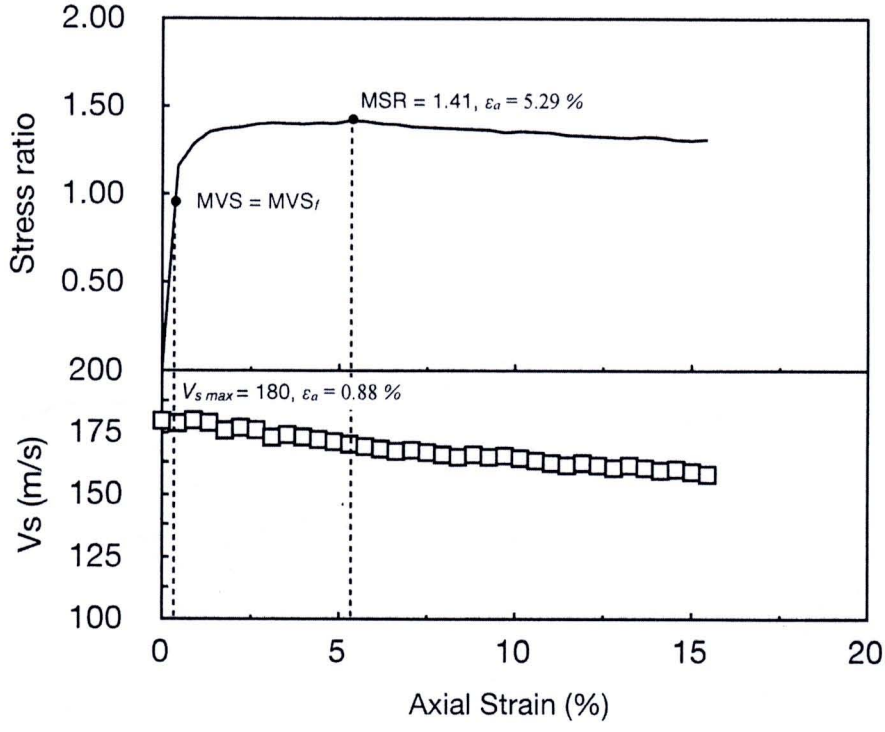

Figure 4.37 The stress ratio and shear wave velocity (V_s) against strain for Silica sand in loose condition with confining pressure 25 kPa

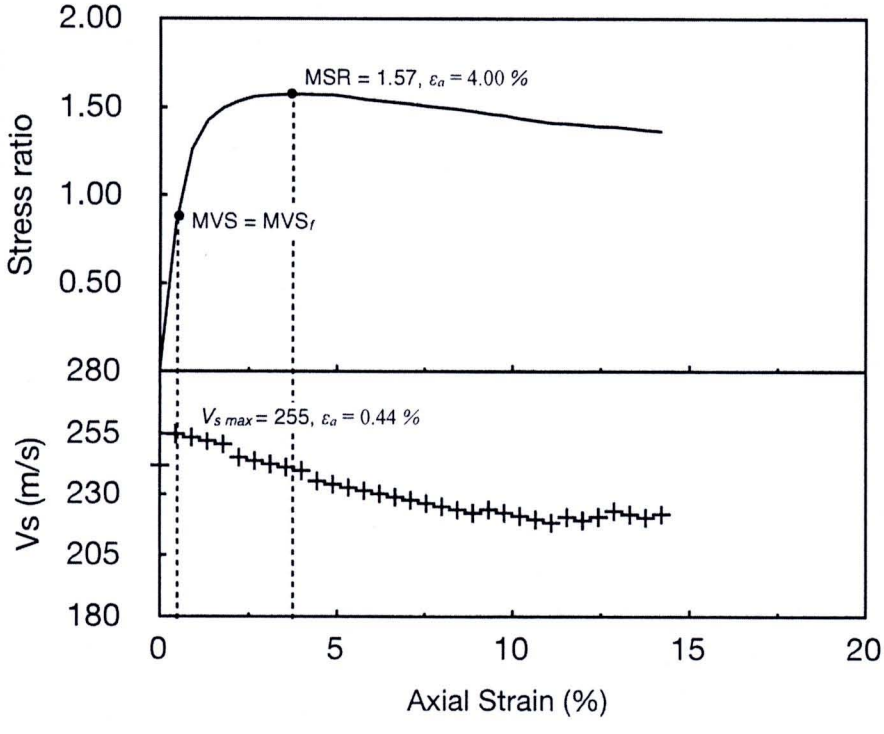

Figure 4.38 The stress ratio and shear wave velocity (V_s) against strain for Silica sand in dense condition with confining pressure 80 kPa

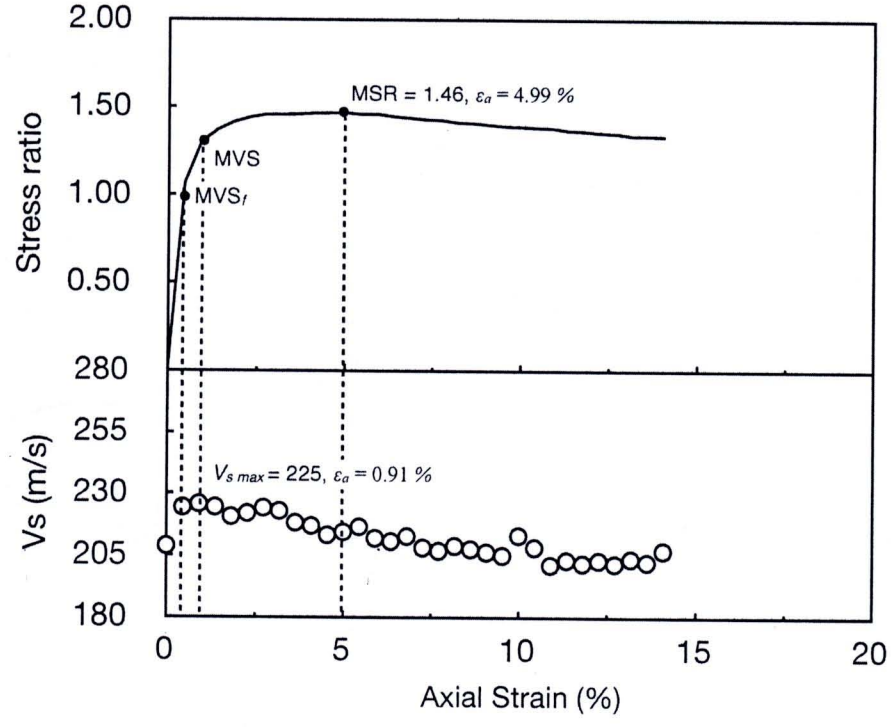

Figure 4.39 The stress ratio and shear wave velocity (V_s) against strain for Silica sand in dense condition with confining pressure 50 kPa

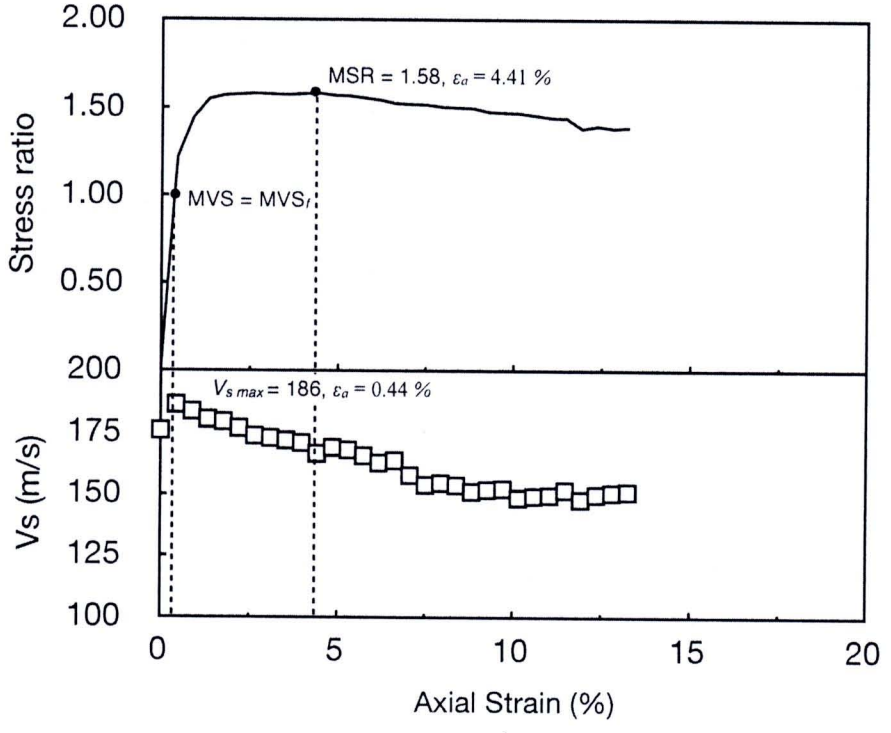

Figure 4.40 The stress ratio and shear wave velocity (V_s) against strain for Silica sand in dense condition with confining pressure 25 kPa

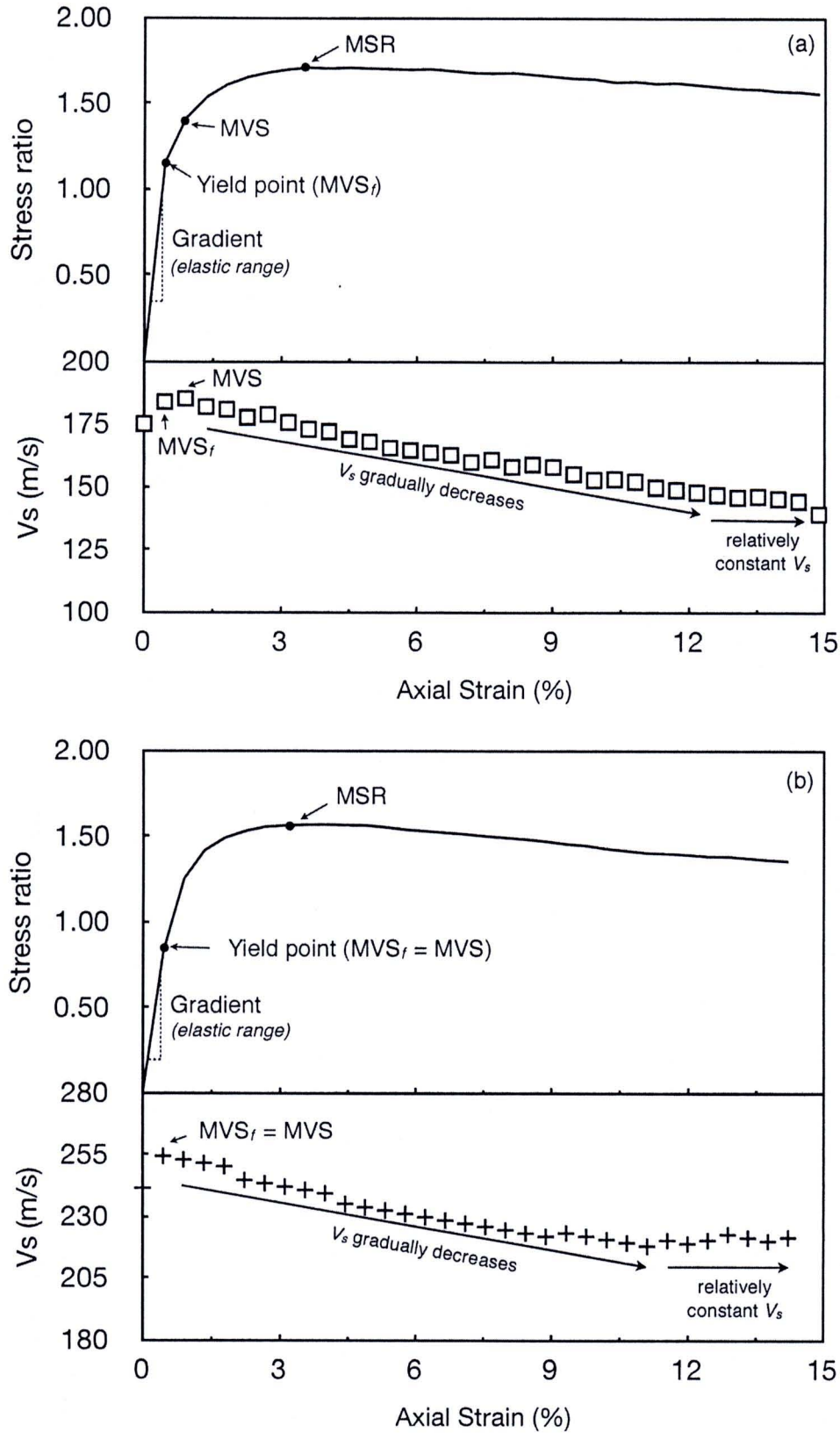

Figure 4.41 The typical results stress-strain and the profile of V_s propagation inside sample during the compression test a) angular-shape and b) round-shape sands

4.3.2 Observation from Digital Image Analysis (DIA) technique

It can be seen from the previous section that although V_s profile can reveal some strain localization characteristics inside the soil sample but the observation of this phenomenon by using DIA would be clearly understand. The measurement of an alteration of grid dimension on the surface membrane of the specimen was performed to observe the local strain distribution inside the deformed sample. This measurements are used to demonstrate how the local elements throughout triaxial specimens of uniform sand evolves during undrained axial compression loading. To compute this local strain profile, the high-resolution of the captured images, i.e. 6 million pixels, would be zoomed in computer software to magnify and precisely determine the deformed size of local elements. The local strain analysis would be based on photo analysis of images taken from a fixed viewpoint at different times during the loading process. The deformation of each local element can be directly calculated by the differentiation between the original length to the deformed length of successive pairs of photographs. The shortest length which can be measured from the magnified high-resolution image is about 0.01 mm.

Two series of local strain analysis by DIA were carried out. The first DIA was performed to observe the zone of strain localization as well as the initiation time of localization in terms of global axial strain. The computation of local axial strain of each element within 3 columns throughout entire height of the specimen will be operated (Fig. 4.42, 4.44, 4,46 4.48, 4.50 and 4.52). The second DIA was done to observe soil non-uniformity and the local strain profile inside the specimen especially in the localization zone. Nine local elements would be randomly selected and calculated the local axial strain. This local strain profiles would then plotted against global axial strain to help in identifying the initiation and evolution of strain localization of sand in triaxial compression tests (Fig. 4.43, 4.45, 4.47 4.49, 4.51 and 4.53). Six sand samples, i.e. D16 of loose and dense packing conditions with confining pressure of 25 and 80 kPa and Silica sand of loose and dense condition with confining pressure of 80 kPa, were selected to observe the evolution of local strain profiles by using DIA technique.

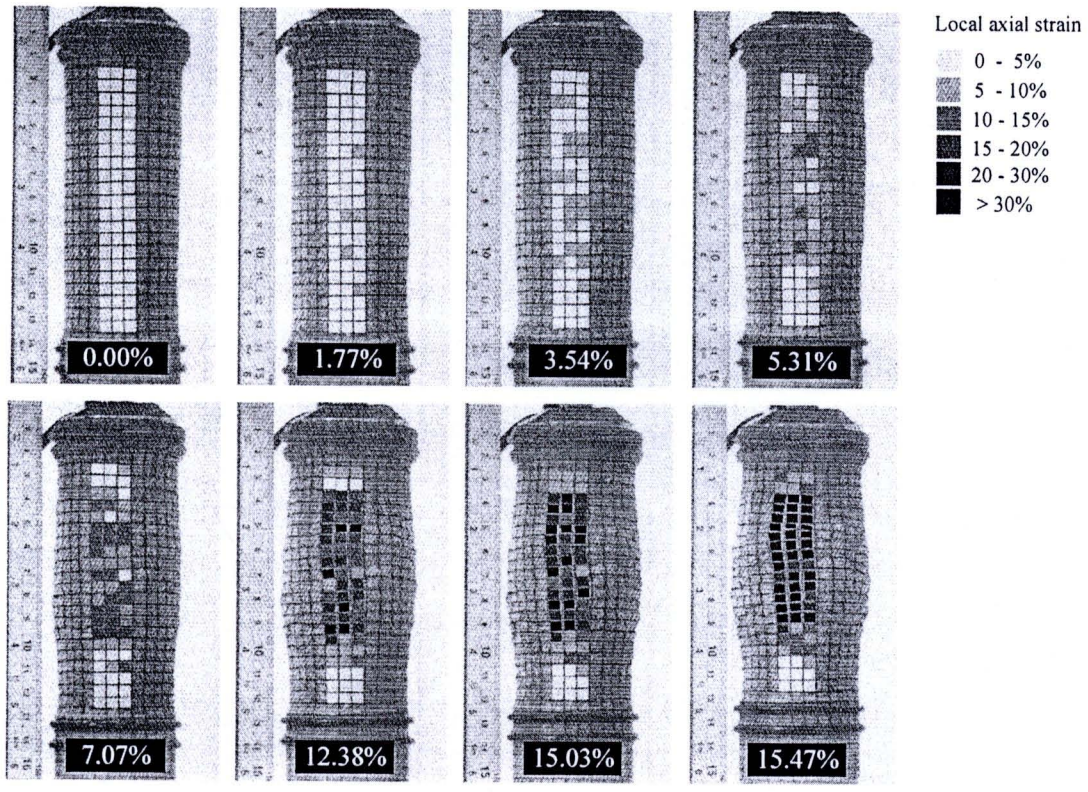

Fig. 4.42 Evolution of local axial strain profile during axial compression loading of D16 sample in loose condition with confining pressure 25 kPa

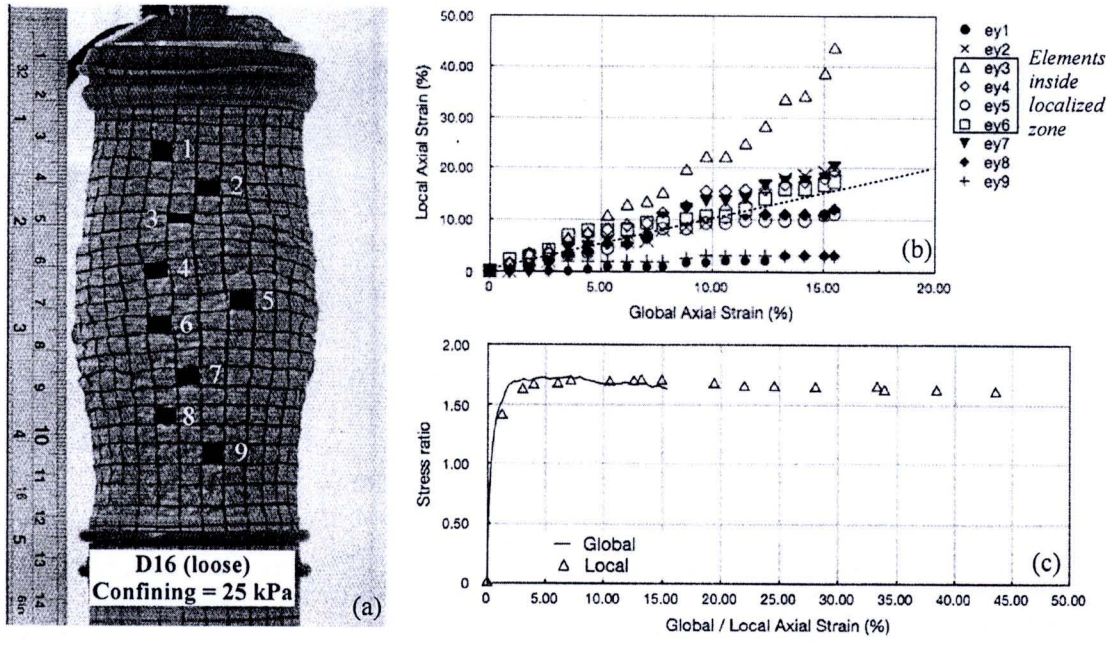

Fig. 4.43 (a) Failure specimen and selected local elements (b) relationship between local and global axial strain (c) stress ratio of the highest deformed element of D16 sample in loose condition with confining pressure 25 kPa

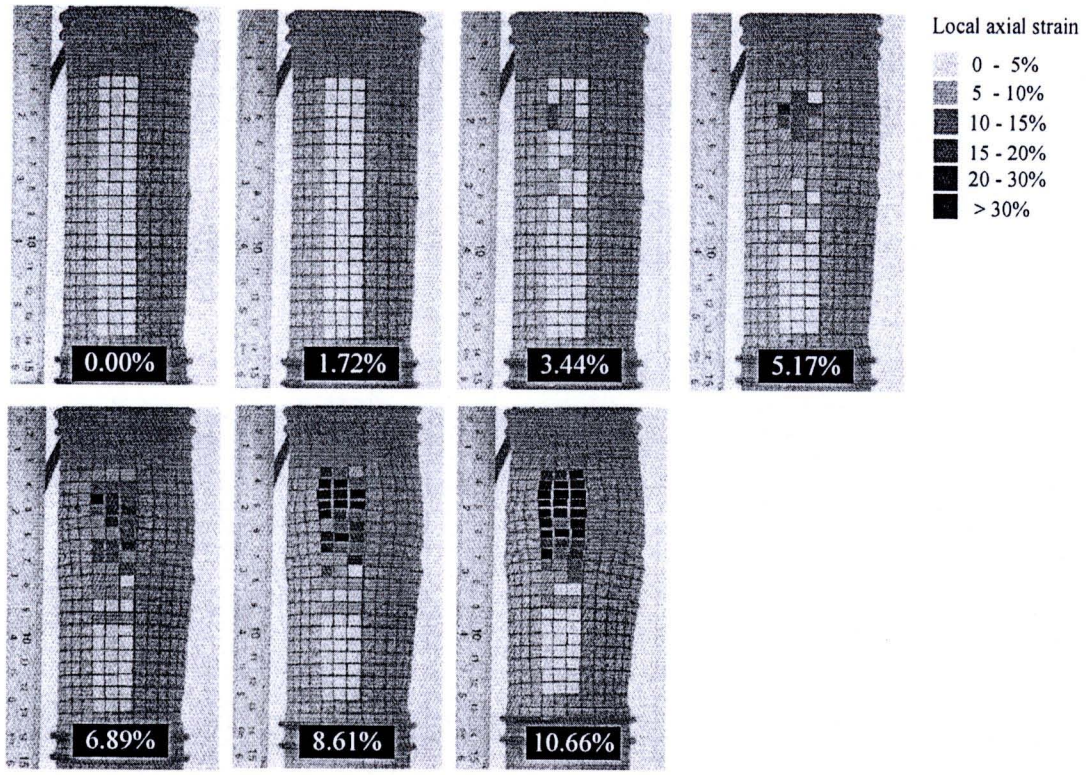

Fig. 4.44 Evolution of local axial strain profile during axial compression loading of D16 sample in dense condition with confining pressure 25 kPa

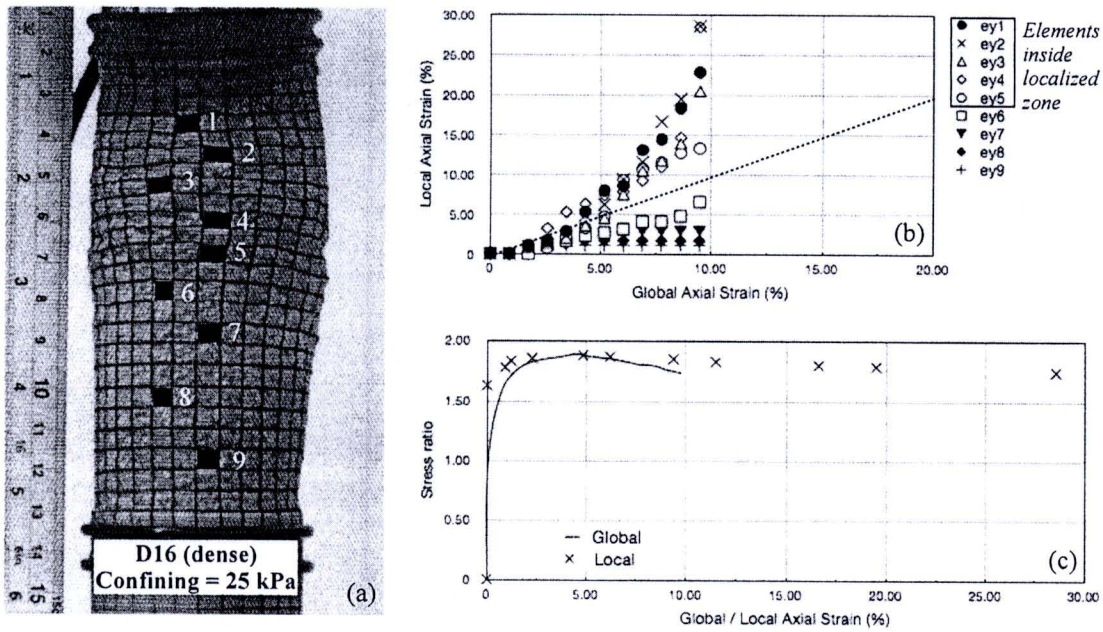

Fig. 4.45 (a) Failure specimen and selected local elements (b) relationship between local and global axial strain (c) stress ratio of the highest deformed element of D16 sample in dense condition with confining pressure 25 kPa

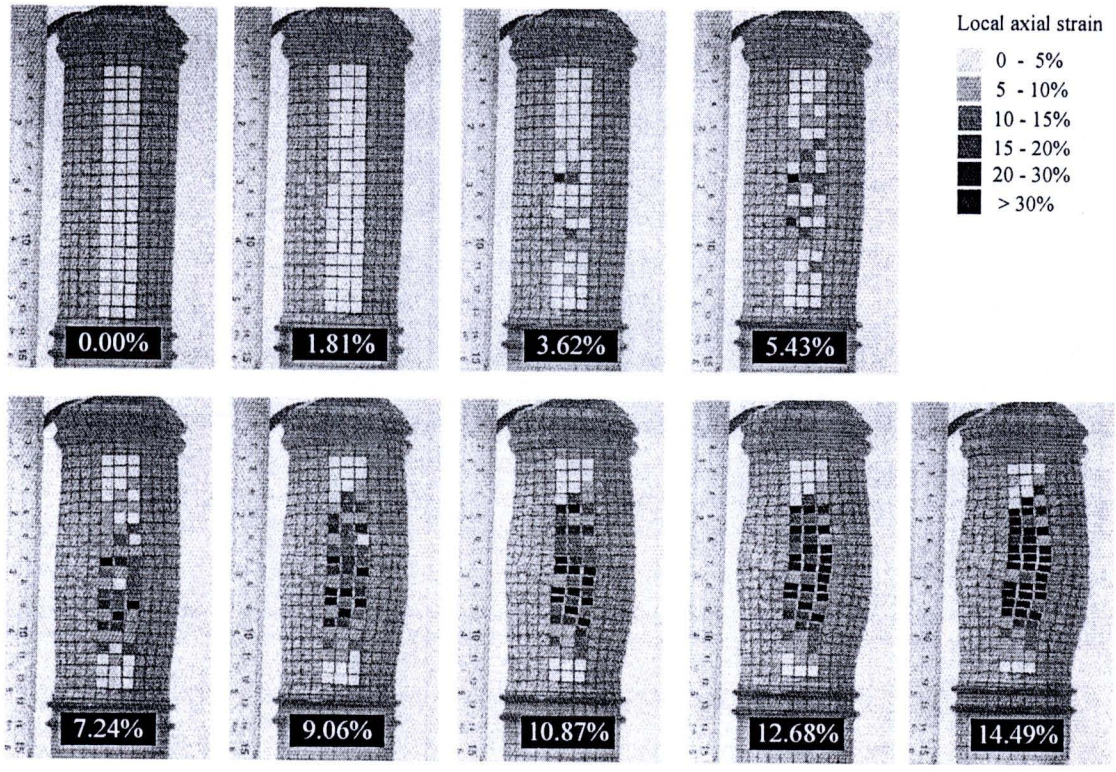

Fig. 4.46 Evolution of local axial strain profile during axial compression loading of D16 sample in loose condition with confining pressure 80 kPa

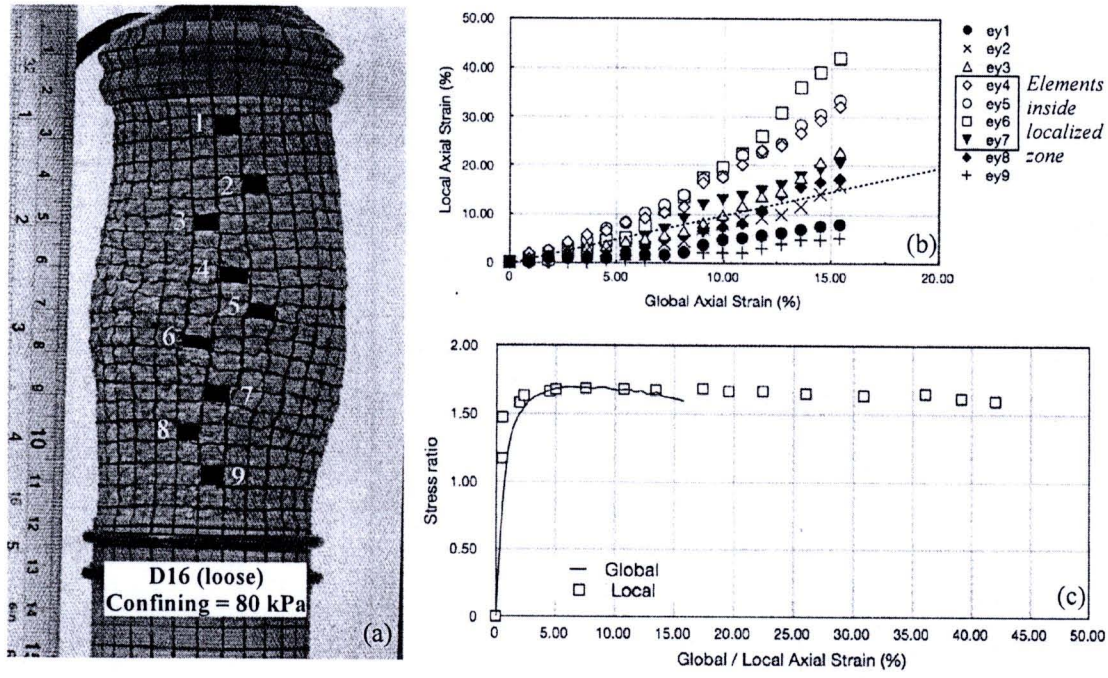

Fig. 4.47 (a) Failure specimen and selected local elements (b) relationship between local and global axial strain (c) stress ratio of the highest deformed element of D16 sample in loose condition with confining pressure 80 kPa

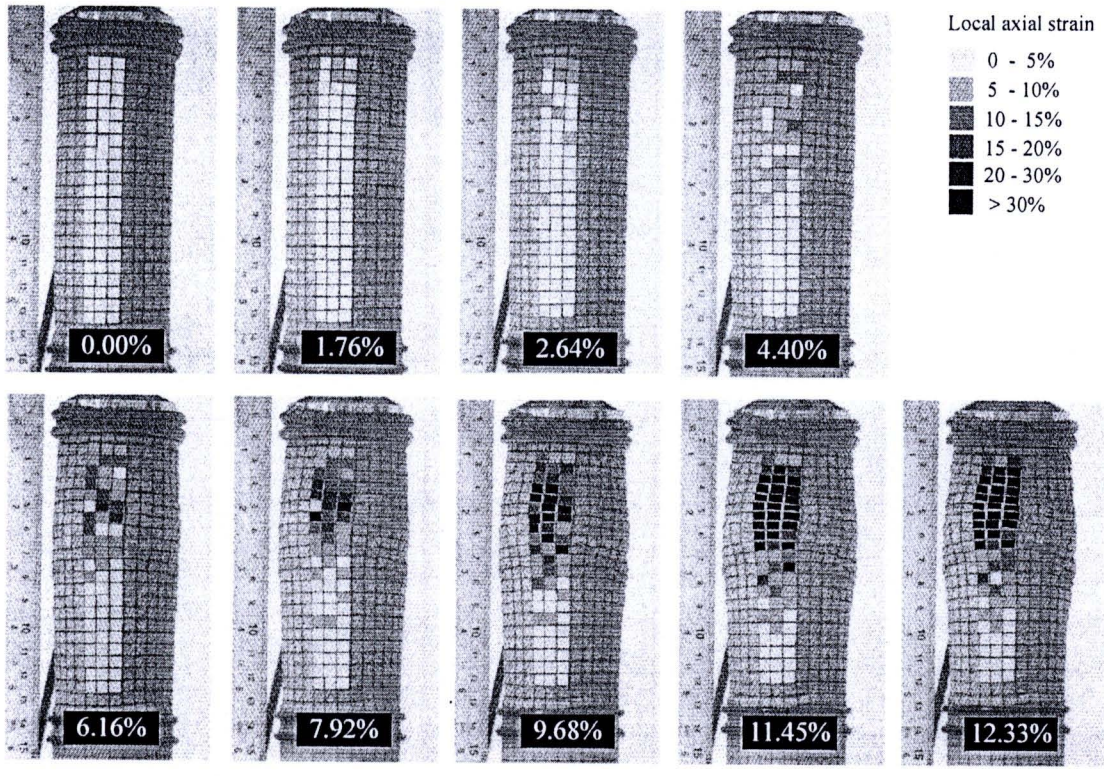

Fig. 4.48 Evolution of local axial strain profile during axial compression loading of D16 sample in dense condition with confining pressure 80 kPa

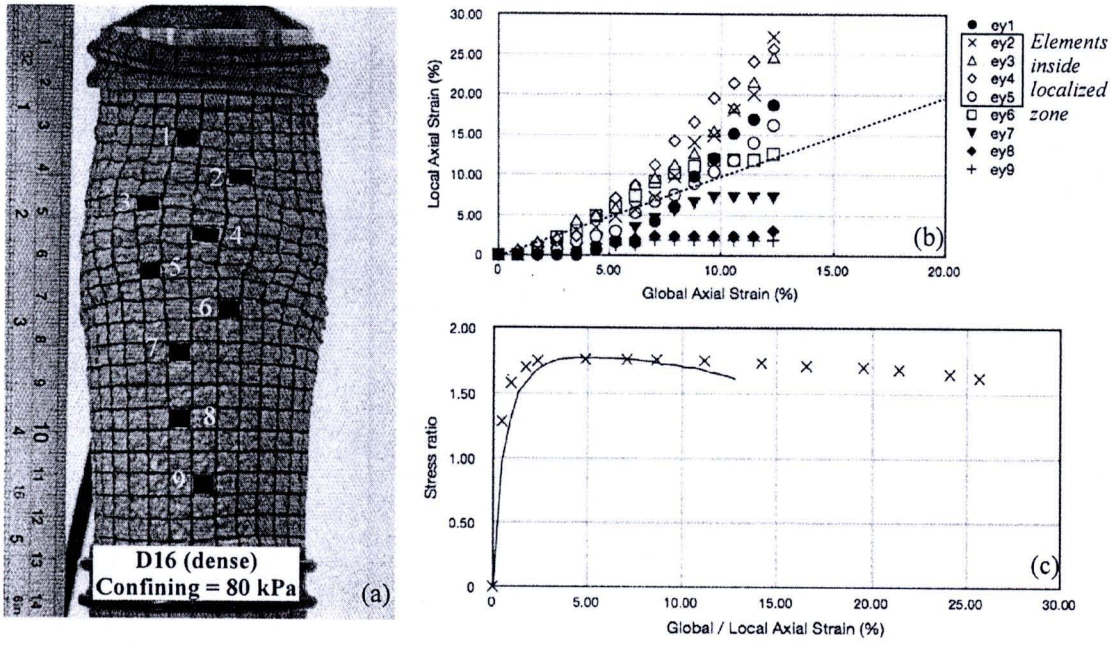

Fig. 4.49 (a) Failure specimen and selected local elements (b) relationship between local and global axial strain (c) stress ratio of the highest deformed element of D16 sample in dense condition with confining pressure 80 kPa

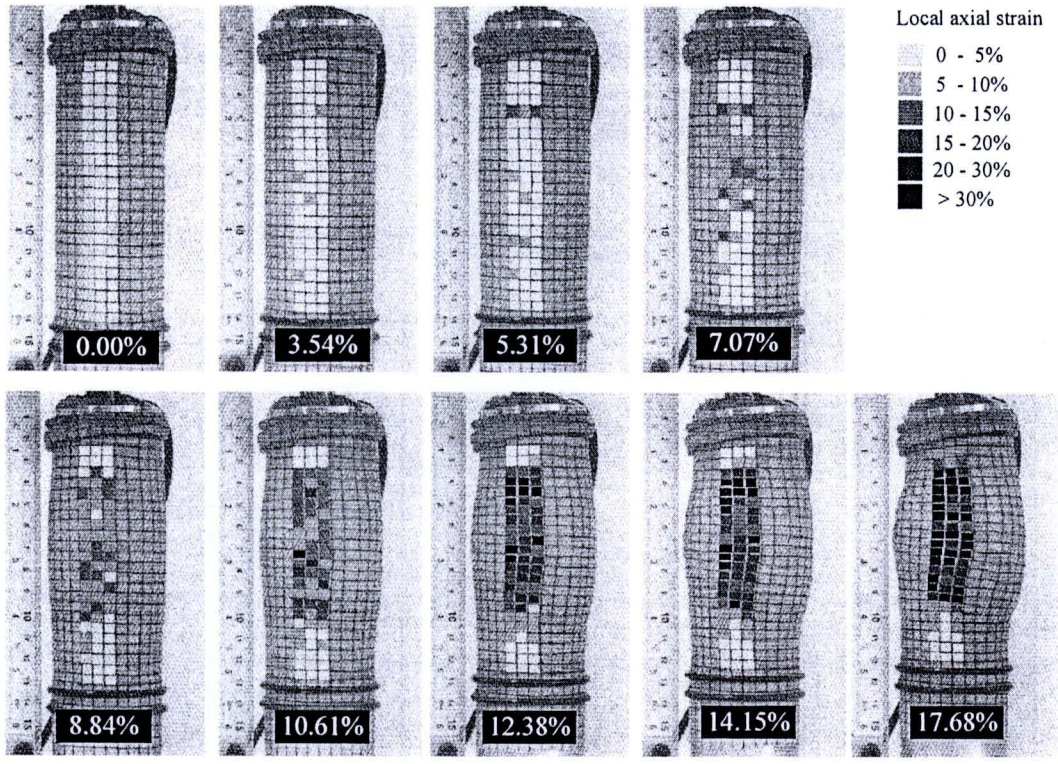

Fig. 4.50 Evolution of local axial strain profile during axial compression loading of Silica sample in loose condition with confining pressure 80 kPa

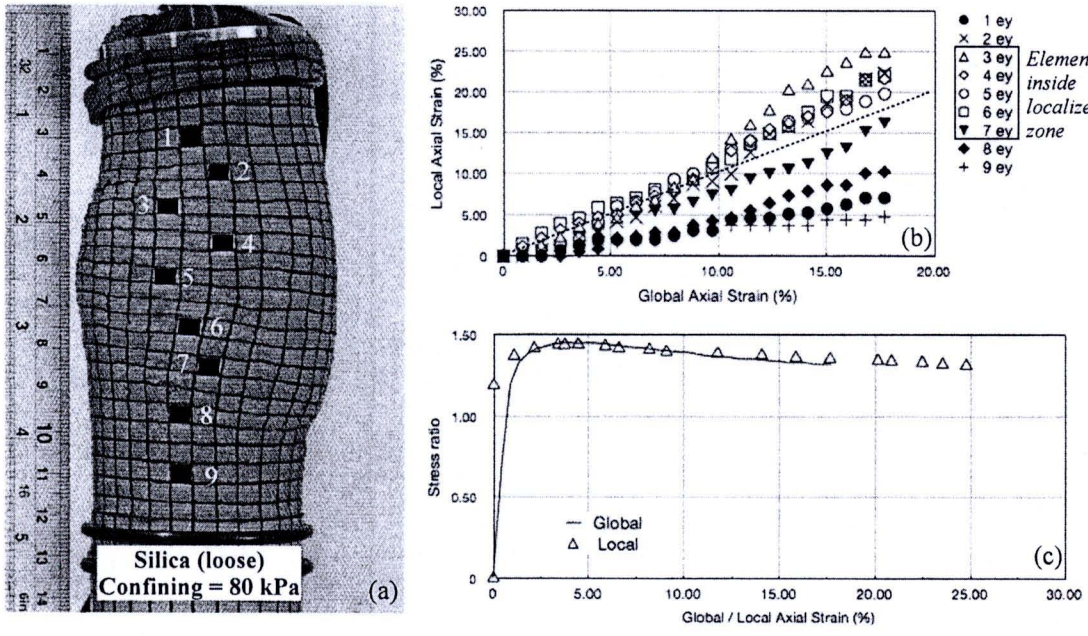

Fig. 4.51 (a) Failure specimen and selected local elements (b) relationship between local and global axial strain (c) stress ratio of the highest deformed element of Silica sample in loose condition with confining pressure 80 kPa

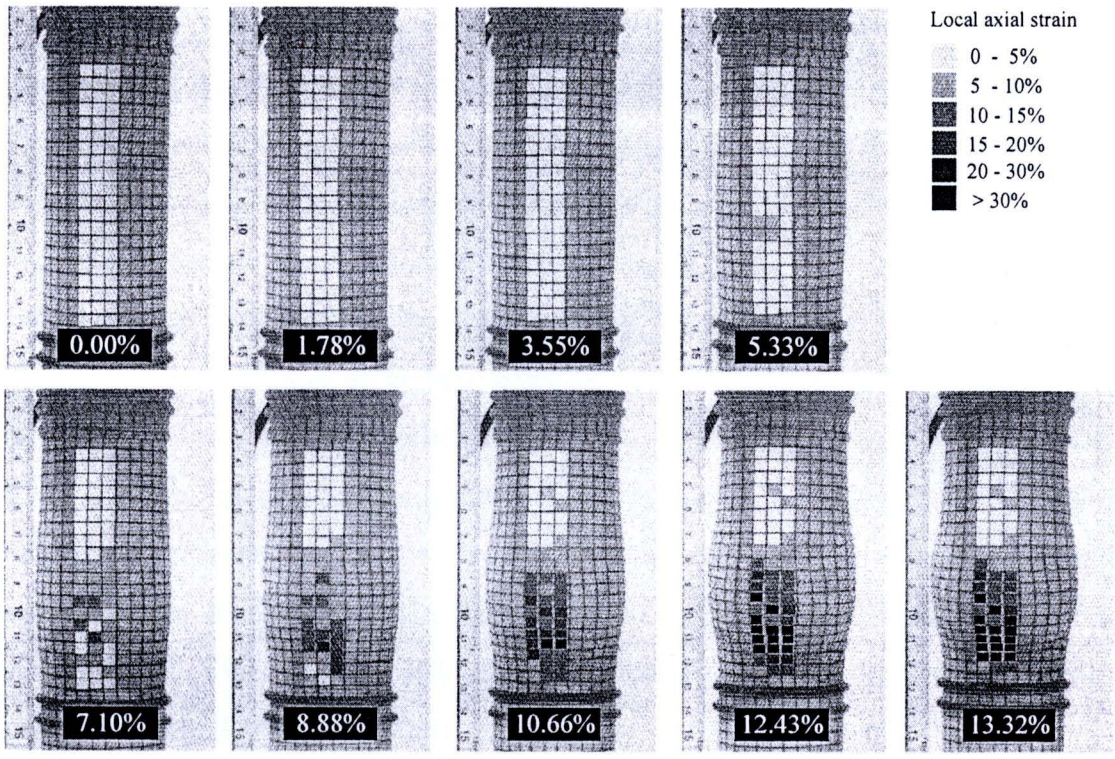

Fig. 4.52 Evolution of local axial strain profile during axial compression loading of Silica sample in dense condition with confining pressure 80 kPa

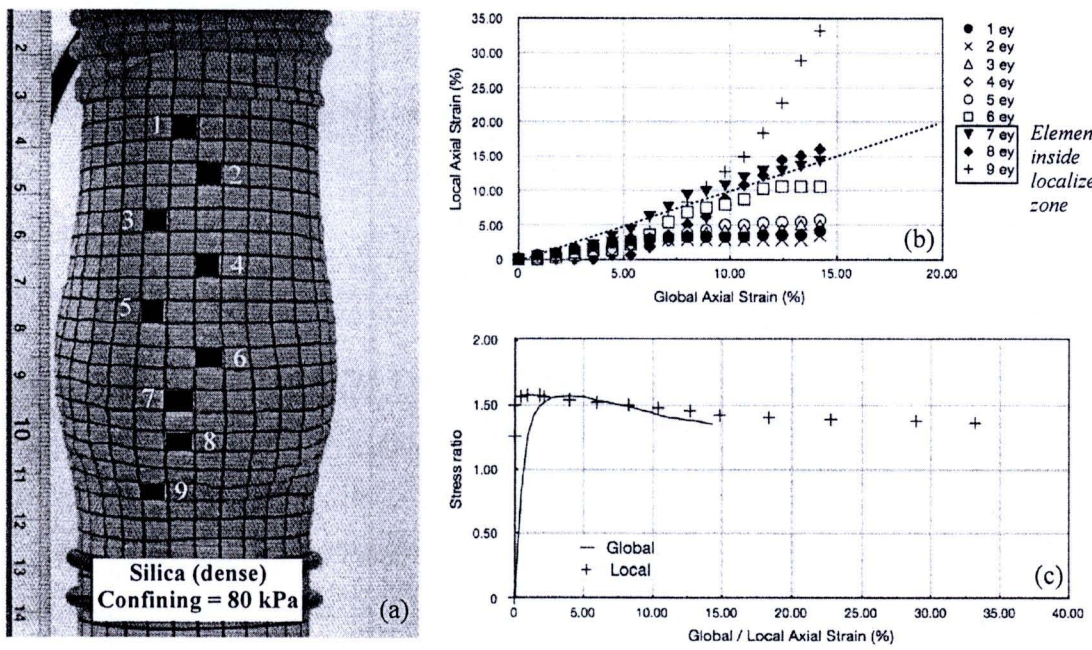

Fig. 4.53 (a) Failure specimen and selected local elements (b) relationship between local and global axial strain (c) stress ratio of the highest deformed element of Silica sample in dense condition with confining pressure 80 kPa

Using the data from digital images, the strain profiles on the surface membrane of the soil specimen could be calculated based on the deformation during the triaxial compression. The strain profiles were developed to illustrate the evolution of localization inside the soil sample. These profiles can explain visually the potential for the initiation of strain localization. In these strain profiles, such as those shown in Fig. 4.42, the vertical strain on the surface of the specimen is displayed and the intensity of gray color at certain point of strain of the profiles represents the magnitude of corresponding axial strain. Fig. 4.42 shows the deformation profile of loose D16 sand specimen sheared under triaxial compression loading conditions at the confining pressure of 25 kPa, which includes the images of specimen and corresponding local axial strain plots at different global axial strain values. The measurement of this variation of local strains could lead to the study of the shear band development and formation within the specimen. In Fig. 4.42, it could be seen that at about 1.77% of global axial strain some local elements of D16 sample exhibit the higher strain (> 5%) than the rest. This strain non-uniformity occurs randomly throughout the specimen. At 3.54% of global axial strain, the sample shows more strain non-uniformity especially at the central portion. Moreover at global strain of 5.31% and so on, this strain non-uniformity develops to form zones of strain localization and these zones distribute along the middle portion of the specimen. It can also be observed that during the entire compression loading the elements outside the localized zone response relatively less value of strain, i.e. < 5%.

Fig. 4.43 also shows the visual inspection of the images of failure specimen and the evolution of local axial strain against global strain. This plot can help in pointing out non-homogeneous of deformation within the specimen. Fig. 4.43(b) shows the progression of local axial strain of selected local elements as in Fig. 4.43(a) against global strain until failure. It can be perceived from Fig. 4.43(b) that elements in the localized zone collect most of the deformation inside the specimen. At failure, the local axial strain of element 3 responses almost 3 times global axial strain. Other elements inside localized zone, i.e. element 4 and 6, also response high value of strain. However, the distribution of axial strain of local elements along the sample is rather uniform. Fig. 4.43(c) shows relationship between the stress ratio versus global /

local axial strain of the highest deformed element inside localized zone. It can be seen that the stress ratio of the highest deformed local element moves along the same path with the global deformation.

Fig. 4.44 shows the evolution of local axial strain profile during axial compression loading of D16 sample in dense condition with confining pressure 25 kPa. The images of local strain profile show that the soil non-homogeneous deformation starts to occur at about 3.44% of global strain and zone of localization fully develops at 5.17% of global axial strain. Comparing to the previous sample of loose packing condition, it might be inferred that dense specimen delayed the strain non-uniformity inside the soil sample. Moreover zone of strain localization of dense specimen is comparatively narrower than loose specimen. Fig. 4.45 also displayed that local axial strain of the highest deformed elements inside the zone of localization have the strain value of nearly 3 times the global axial strain. This behavior confirms a higher deformation characteristic inside the localization zone. The figure also shows that the distribution of strain of local elements along the height of the sample is not uniform as in the loose specimen. The alteration of local strain value of some local elements, i.e. elements 1, 2 and 4, shifts rapidly especially after the onset of soil non-homogeneous (Fig. 4.45b). The stress ratio of the highest deformed local element almost moves along the same path with the global deformation (Fig. 4.45c). Fig 4.46 to 4.53 show the DIA results of D16 and Silica samples in loose and dense conditions with confining pressure of 80 kPa. The similar outcomes could also be attained for these types of samples and testing conditions.

Both observations, i.e. by shear wave velocity profile and DIA, could clarify some important characteristics of strain localization to some extent. Therefore, to explicitly explain the initiation and evolution of strain localization behavior, the pictures illustrating those results from the previous findings would be showed again in Fig. 4.54 to Fig. 4.59. Fig. 4.54 is the comparison results of the stress ratio, shear wave velocity and local strain profile of D16 sample in loose condition with confining pressure 25 kPa. Point a on the stress ratio curve corresponds to the second picture of local strain profile at 1.77% of global axial strain. If we look at the point of maximum V_s at 1.32% of global axial strain, we will see that after this point of $V_{s(max)}$ the onset

of strain non-uniformity inside the specimen will occur. This point of non-uniformity deformation can be confirmed by the appearance of some local elements exhibiting vertical strain to more than 5%. From these figures, it can also be noticed that at the point of maximum stress ratio (MSR) the zone of strain localization will be fully developed (point c).

Fig 4.55 shows the comparison results between stress ratio, shear wave velocity profile and local strain profile of D16 sample in dense condition with confining pressure 25 kPa. Point a on the stress ratio curve is at 3.44% of global strain, at this point some local elements response to non-homogeneous deformation, i.e. >5%, and occurs after the point of maximum shear wave velocity. Point b is the point where the zone of localization is fully progressed and occurs nearly the point of maximum stress ratio. These relevant consequences could be discerned for the tests on D16 sample with loose and dense packing conditions with confining pressure 80 kPa. (Fig. 4.56 and Fig.4.57). However, for Silica sand of loose and dense conditions with confining pressure 80 kPa, the behavior of strain localization from shear wave velocity profile and local strain profile by DIA is not corresponding to each other. Namely, V_s tends to decrease from its maximum value at the very beginning of the test, e.g. 0.88%. However, local strain profile by DIA do not show any non-uniformity deformation within the specimen at this value of global axial strain. The non-uniformity deformation, observing from DIA, starts at about 3.54% and 5.33% of global axial strain for loose and dense sample of Silica sand, respectively. Though DIA can be easily performed to study the strain localization but there are still some limitations and accuracies. On the other hand, shear wave propagation technique can still detect that point of non-uniformity within the soil specimen comprehensibly.

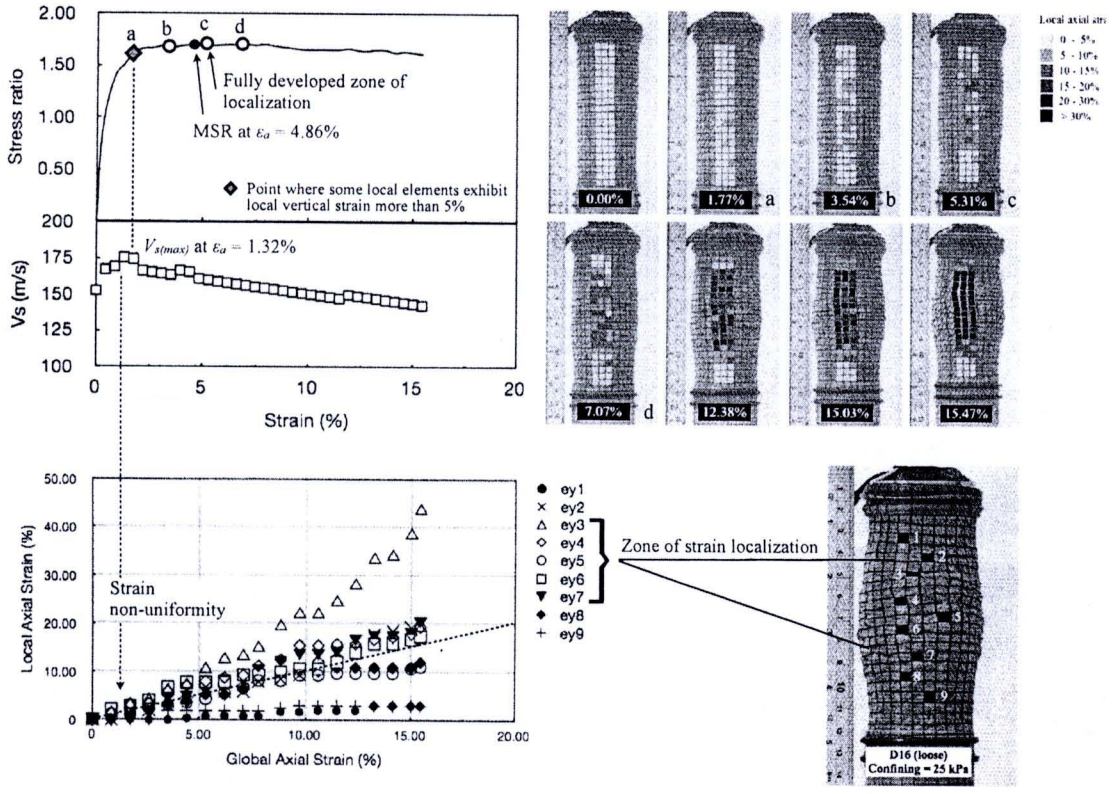

Fig. 4.54 The stress ratio, shear wave velocity and local strain profile of D16 sample in loose condition with confining pressure 25 kPa

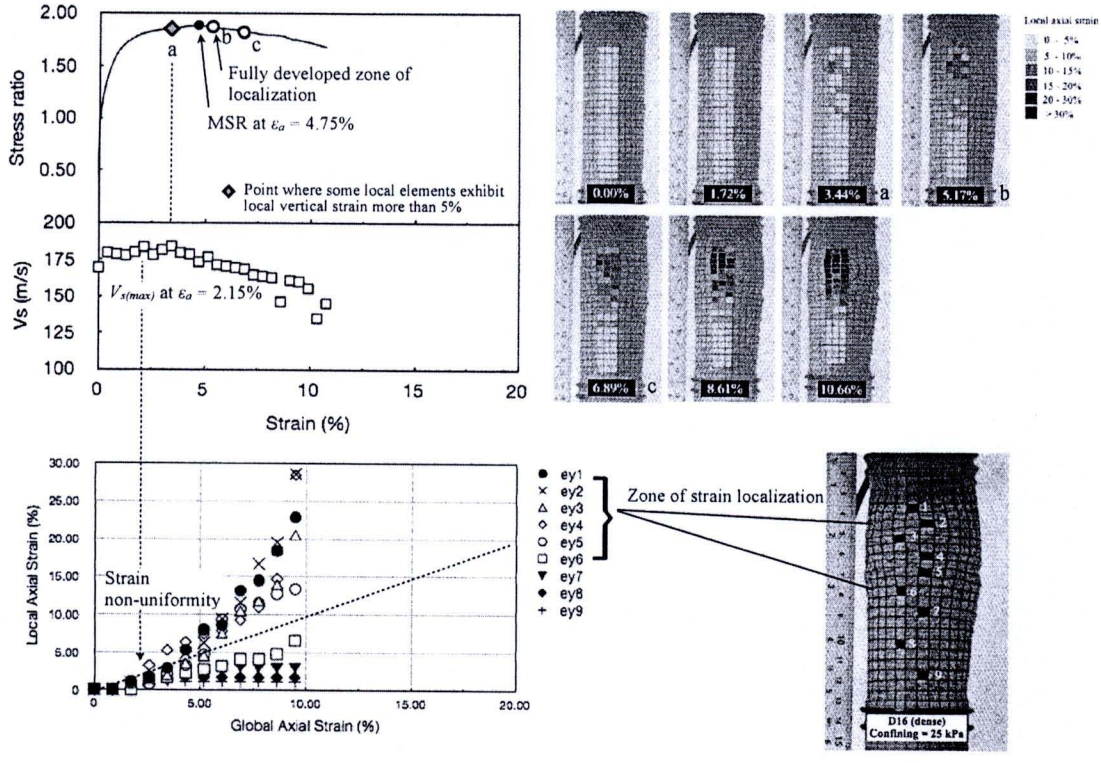

Fig. 4.55 The stress ratio, shear wave velocity and local strain profile of D16 sample in dense condition with confining pressure 25 kPa

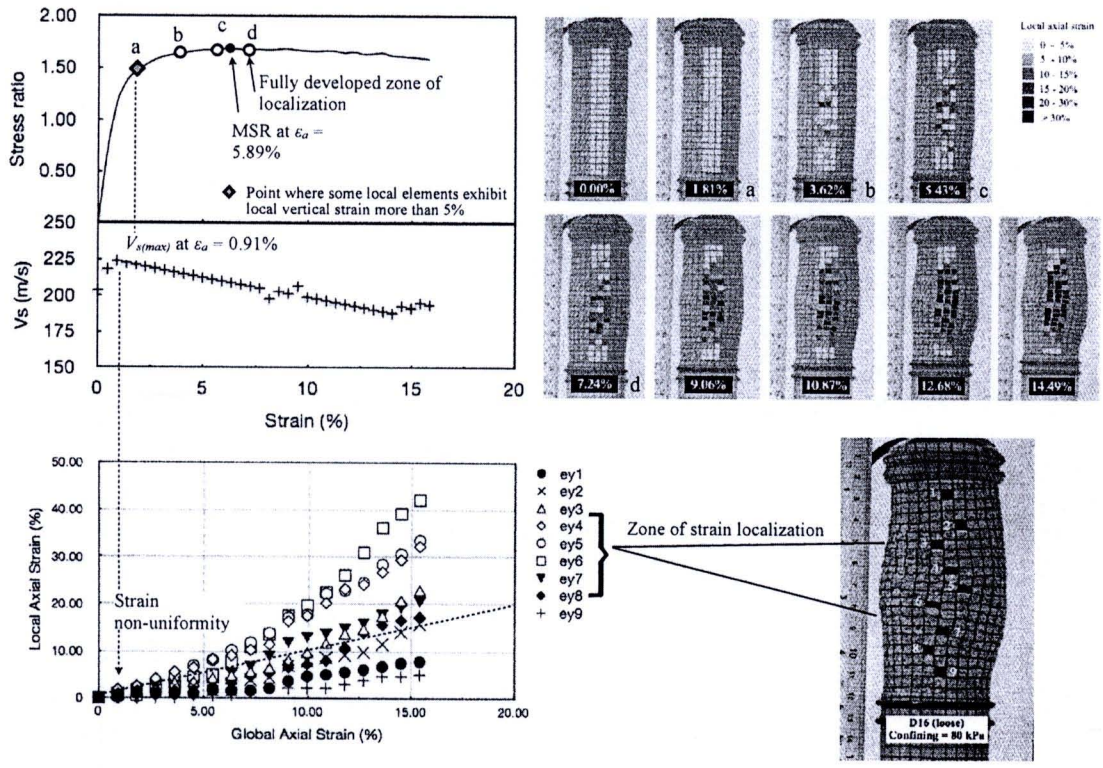

Fig. 4.56 The stress ratio, shear wave velocity and local strain profile of D16 sample in loose condition with confining pressure 80 kPa

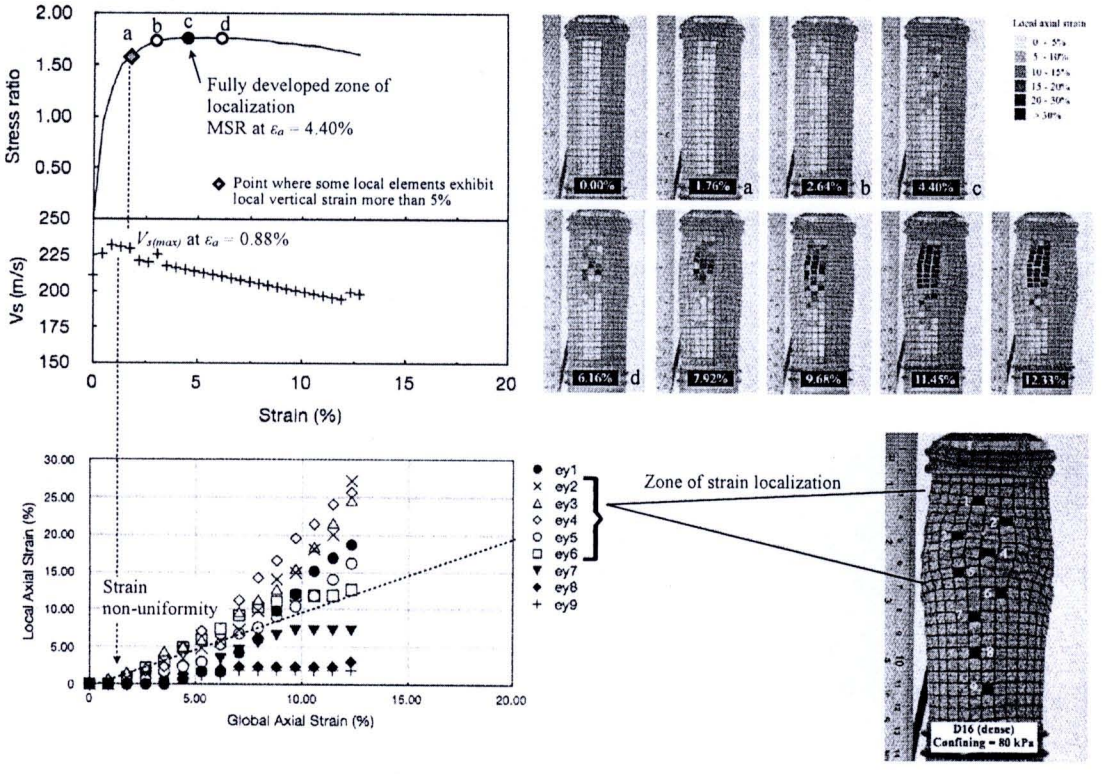

Fig. 4.57 The stress ratio, shear wave velocity and local strain profile of D16 sample in dense condition with confining pressure 80 kPa

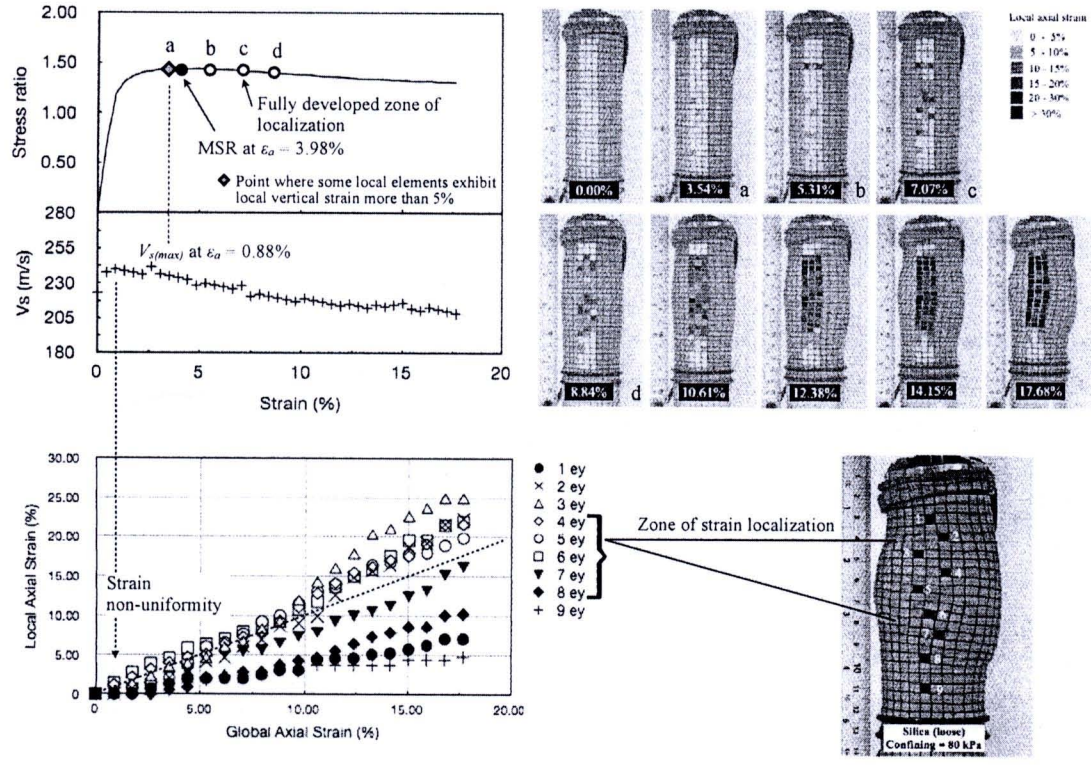

Fig. 4.58 The stress ratio, shear wave velocity and local strain profile of Silica sample in loose condition with confining pressure 80 kPa

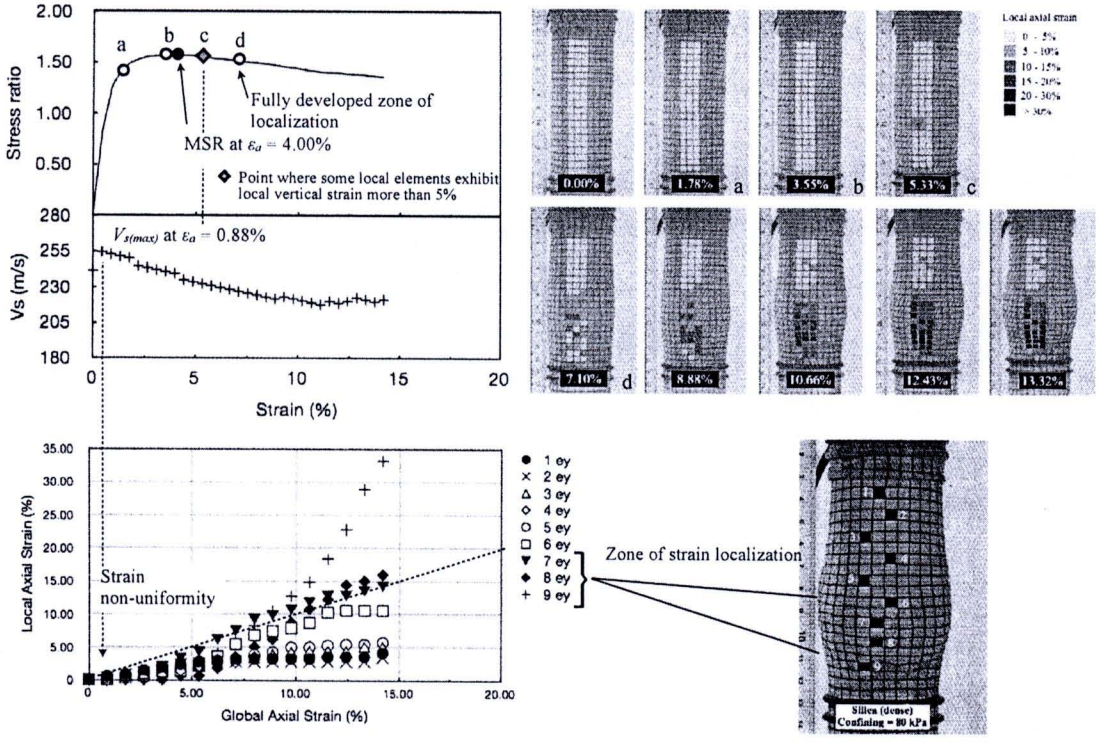

Fig. 4.59 The stress ratio, shear wave velocity and local strain profile of Silica sample in dense condition with confining pressure 80 kPa